Shaking table tests of a full-scale base-isolated flat-bottom steel silo equipped with curved surface slider bearings

SHAKING TABLE TESTS OF A FULL-SCALE BASE-ISOLATED FLAT-BOTTOM STEEL SILO EQUIPPED WITH CURVED SURFACE SLIDER BEARINGS

Marco Furinghetti[1,2], Sulyman Mansour[3], Matteo Marra[4], Stefano Silvestri[4], Igor Lanese[2], Felix Weber[5], Alberto Pavese[1]

[1] Department DICAr, University of Pavia, Pavia, Italy

[2] EUCENTRE Foundation, Pavia, Italy

[3] Department DICAR, Polytechnic University of Bari, Bari, Italy

[4] Department DICAM, University of Bologna, Bologna, Italy

[5] Maurer Switzerland GmbH, Pfaffhausen, Switzerland

Correspondence:

Marco Furinghetti

marco.furinghetti@unipv.it

ABSTRACT

This paper presents a series of shaking table tests on a full-scale flat-bottom steel silo filled with soft wheat, under isolated-base conditions. The tested specimen is a 3.64 m-diameter 5.50 m-height corrugated-wall cylindrical silo, representing the smallest manufactured silo available in the catalogue of an Italian commercial silo provider. Curved Surface Slider isolators were introduced between the shaking table and the reinforced-concrete plate, on which the silo was mounted, to realize the isolated configuration where the main results have been investigated and compared with other results for the same silo specimen under fixed-base conditions. A detailed description of the silo components, the filling bulk material properties as well as the test setup is provided, including the full testing protocol. Multiple sensors were used to monitor the dynamic response of the filled silo system, including accelerometers, pressure cells, LVDT displacement transducers. Numerous unidirectional dynamic tests were conducted consisting of random signals, sinusoidal inputs, pulse-like inputs, and both artificial and real earthquake records. The results were processed to evaluate the performance of the isolators and their effectiveness on the silo response in terms of measured accelerations and dynamic overpressures. The efficiency of the isolation on the reduction of both acceleration amplifications over the silo wall height as well as the captured dynamic overpressures were detected in the range 30%-80% depending on the input type and magnitude.

KEYWORDS

Silo, earthquake, granular material, shaking table, isolator, curved surface slider, frequency.

1 INTRODUCTION

Industrial silos are commonly used structures for the storage of bulk products. Different materials can be stocked in storage units whose use varies from human consumable food products (e.g., wheat, rice, corn, etc.) to chemical and industrial substances (coal, powders, etc.). The content, the conditions as well as the operation processes of the industrial facility in which the silo structure is built have a strong impact on the selected construction material, the design requirements, the health monitoring strategies and protection plans. ([1]; [2]; [3]; [4]).

Modern silos are mainly constructed in steel, rather than reinforced concrete as in the past, exploiting the advantages of the relatively low weight of the structure, reducing the costs, and improving the building conditions in terms of time and accuracy. Silos, whether made of steel (either of flat or corrugated wall section) or reinforced concrete, are characterized by frictional surfaces governing the interaction between the stored granular material and the surrounding wall and the base ([5]; [6]). The interaction of the granular solid with the base represents an essential difference between flat-bottom and elevated silos, which leads to a complicated behavior of the flat bottom silos under seismic excitation. On one hand, for the elevated columns-supported silos, the whole stored material could be represented by a mass at the upper end of cantilever beam leading to a well-known dynamic behavior (e.g., idealized SDOF system). On the other hand, for the flat-bottom ground-supported silos, the mechanical behaviour of the filled silo system is still not fully understood (mainly for silos characterized with squat filling conditions [7]; [8]; [9]; [10]; [11]).

Several earthquake events have been observed in the last 40 years, and their consequences on industrial facilities and silos have been investigated ([12]; [13]; [14]; [15]; [16]; [17]; [18]; [19]; [20]; [21]; [22]; [23]). That was accompanied by increasing interest in the seismic behavior of silo systems, since the damages vary in terms of human, economical, and even political costs in relation with the function and importance of the vital industrial complex. Such a recent global trend has been evolving toward different directions: 1- understanding the seismic behavior of the filled silo systems through theoretical, numerical ([24]; [25]; [26]; [27]; [28]) and experimental studies ([29]; [30]; [31]; [32]; [33]; [34]; [35]; [36]; [37]; [38]; [39]; [40]; [41]; [10]; [11]); 2- evaluating the seismic vulnerability of existing silos to assess their current level of risk ([42]; [43]; [44]; [39]; [45]; [46]; [47]; [48]) and 3- protecting new and old silos by means of improving the seismic response of silo itself, or the silo battery either by introducing seismic dissipation ([49]) or isolation devices ([50]; [51]; [52]; [53]; [54]; [55]). In this regard, experimental testing, and specifically at the actual scale, is still very limited due to high complicated technical requirements and economic difficulties, leading the research development towards the analytical and numerical direction, resulting in unavoidable uncertainties in the findings.

The work presented here is concerned with the introduction of seismic isolation devices at the base of a filled silo system, in which an actual industrial flat-bottom silo is filled with wheat and mounted on a reinforced concrete slab on the top of a shaking table. The choice of the seismic isolation system might represent a reasonable technical solution that can be introduced below the reinforced concrete foundation plate of a single silo or a silo battery due to the following reasons: (1) to overcome the uncertainties related to the lack of full understanding of the seismic response of flat-bottom ground-supported silos; (2) to keep the silo superstructure in the elastic field, thus ensuring its functionality by avoiding excessive deformations; and (3) to provide a first attempt to extend the benefits

highlighted by the promising numerical and experimental studies available in the literature in the field of liquid storage tanks to the field of silos filled with granular material ([56]; [57]; [58]; [59]; [60]; [61]; [62]; [63]; [64]; [65]; [66]; [67]; [68]; [69]).

In the recent past some research works can be found in the scientific literature, about the definition of the seismic isolation system for storage tanks rather than industrial structural systems ([70], [71]). Even though some data are available on the topic, the overall behavior of such structural systems has to be widely investigated through both numerical and experimental analyses ([72], [73]). For instance, one of the very first assumption for the proper design of the isolation system of a storage tank is represented by the choice of the isolation device technology, among the available isolators used in the common practice: namely Rubber Bearings with or without a central dissipative Lead core (RB [61, 68] and LRB [56, 65] respectively) and Curved Surface Slider devices (CSS) [58-61, 64, 66]. The adoption of the optimal isolation technology is a key issue for the most effective reduction of the seismic vulnerability of a SILO structural system, and a number of aspects have to be considered in detail, not only from the mechanical perspectives, but also from the sustainability and maintenance standpoints. Recently some research works dealt with the response of industrial facilities, seismically protected by means of base-isolation systems, based on Lead Rubber Bearings and low-damping isolators, and interesting outcomes have been highlighted ([74], [75]). However, in real applications generally a large number of laying points may be needed to support the overall structure and consequently hybrid systems are expected to be adopted, when rubber-based isolators are used (rubber bearings with low-friction flat sliders). Therefore, Curved Surface Slider devices are expected to be the most suitable solution for the definition of the isolation system, since the whole set of isolators provides the same designed force response characteristics, together with a significant dissipative capacity, induced by the frictional properties.

Within this context, this is the first work presenting an experimental test carried out on a full-scale flat-bottom silo placed over an isolation system under seismic excitation. The tested specimen is a commercial steel silo characterized by a 3.64 m diameter and 5.5 m height, filled with soft wheat as a product. It should be noted that the specimen is an actual silo whose steel elements were transferred to the laboratory and mounted over a reinforced concrete base plate, differently from the commonly used silo representative models in literature. Moreover, the filled material was real wheat which provided an actual stocking case inside the silo (see chapters 4.4 and 5.1 of [11] for further details related to the complicated quasi concentric filling procedure), thus overcoming the usual scaling problems traditionally found in literature. The silo has been tested over a shaking table in two configurations: 1- fixed-base conditions, in order to identify the dynamic properties and seismic response under the effects of a variant of seismic inputs in terms of nature and magnitude (more details in section 4 and in [11]) and 2- isolated-base conditions, under the effect of the same input program of the first testing phase, to evaluate the benefits of introducing the isolation system.

The main objective of this paper, representing the companion paper of [11], is twofold: (i) to provide a detailed characterization of the isolation system, (ii) to discuss the dynamic response of superstructure (filled silo system) and to provide a unique comparison with the same silo in fixed-based conditions. Section 2 describes the silo specimen, filling material, the isolation devices, and equipped measuring sensors. Section 3 details the complete

testing program in both fixed- and isolated-base conditions for comparison motivations. Section 4 collects briefly the main results obtained in the fixed-base configuration, highlighting the differences in the dynamic and seismic responses from the liquid tanks [76]. Section 5 gives an in-depth qualitative and quantitative study of the response of the isolation system is introduced, then it was compared to the expected behavior provided by the available analytical models. Finally, Section 6 reports on the isolated silo response in terms of the registered acceleration profiles and captured dynamic overpressures (i.e., the additional pressures provoked by the dynamic input with respect to the static pressures) during the isolated-base testing session. As expected, the adopted isolation system significantly mitigates both dynamic overpressures and accelerations on the silo superstructure. Thus, the work here tries to put the experimental findings in the suitable scientific context, justifying the results by means of intense qualitative and quantitative comparisons with the original fixed-base configuration results in order to assess the main benefits of the proposed isolation system and its suitability for the seismic protection purposes of such a vital industrial facility.

2 STRUCTURAL SYSTEM

2.1 The steel silo specimen

An actual commercial silo (Figure 1) was selected as a specimen and tested under two configurations: (i) fixed-base [10] and (ii) isolated-base conditions. The specimen is the smallest silo provided by industrial storing silos company, whose diameter is around 3.64 m, and its height is 5.5 m. The silo is built be means of mounting twenty horizontally steel sheets (five rings of four sheets) using bolted connections (three tiers along vertical connections and one row along horizontal connections) and eight vertical Ω-shaped stiffeners. The roof silo instead was collected using 16 flat steel panels with end corrugation and connected with the silo wall by a circumferential ring beam at the top height of the shell wall. The silo was built over a r.c. plate on which the silo fixed at the 8 base points of the stiffeners using base plates with anchor bolts. Four isolators were positioned between the tested system and the shaking table. Aiming at providing the proper connection between the reinforced concrete slab and the silo during motion, special steel anchorage systems have been installed, and consequently no sliding and rocking movements were permitted to occur. The isolated-base configuration has been realized by removing those devices, at the end of the first session of tests, allowing the isolators to be active. Finally, the silo was designed and built to ensure the elastic response of the silo since the ductility behavior is out of the investigation scope. Table 1 reports all technical details of the tested silo structure and sub-structure as well as the stored material.

Table 1: Technical data sheet of the tested filled silo system.

Silo specimen			***Stored product***		
Diameter	[m]	3.64	**Material**	[-]	Soft wheat
Height (shell wall)	[m]	4.4	**Average diameter**	[mm]	2.5 – 3
Height (shell wall + roof)	[m]	5.5	**Unit weight**	[kN/m^3]	8.04
Provider	[-]	AGI EMEA (ex AGI FRAME)	**Internal frictional coefficient**	[-]	0.55
Material	[-]	S350GD	**Friction coefficient with corrugated wall**	[]	0.5
Galvanization	[-]	Z450	**Angle of repose**	[degree]	30
Shell wall			**Humidity**	[%]	30-45
N. of rings	[#]	5	**Average temperature**	[°C]	16
N. of sheets in single ring	[#]	4	***Filling condition***		
Connection type	[-]	Bolted connection	**Filling mode**	[-]	Quasi concentric
Bolts	[-]	M10	**Filling height**	[m]	3.3
Wall section	[-]	Horizontally corrugated wall	**Aspect ratio**	[-]	0.91
Single sheet thickness	[mm]	1	**Slenderness (EN 1991-4)**	[-]	Squat
Single sheet dimensions	[mm]	2857.5 [b] x 881 [h]	***Foundation***		
Wave period	[mm]	67.7	**Foundation type**	[-]	r.c. plate
Wave height	[mm]	13.5	**Slab dimensions**	[m] x [m]	5.5 x 5
Wave radius	[mm]	18	**Slab thickness**	[m]	0.5
Vertical stiffening elements			**Slab material**	[-]	C25
Stiffener elements	[-]	Hat-shaped thin open cross-section stiffener	**Connection with silo**	[-]	Base plates
N. of stiffeners	[#]	8	**N. of base plates**	[-]	8
Stiffener thickness	[mm] per ring (1 from top)	1.5 (r. 1), 2 (r. 2 and 3) and 3 (r.4 and 5)	**Base plate dimensions**	[mm]	400 x 435
Stiffener connections	[-]	67.7 mm spaced bolted seam	**Base plate thickness**	[mm]	10
Bolts	[-]	M10	***Shaking table***		
Stiffeners connection plate thickness	[mm]	3	**Type**	[-]	Unidirectional
Roof detailing			**Dimensions**	[m] x [m]	5.6 x 7.0
Roof structure	[-]	Inclined steel sheets	**Capacity**	[t] per 1 g PTA	100
Roof plate shape	[-]	Omega shaped	***System weight***		

N. of roof plates	[#]	16	**Super-structure**	[kN]	12
Roof plate thickness	[mm]	1	**Sub-structure**	[kN]	230
			Material	[kN]	285
			Total weight	[kN]	527

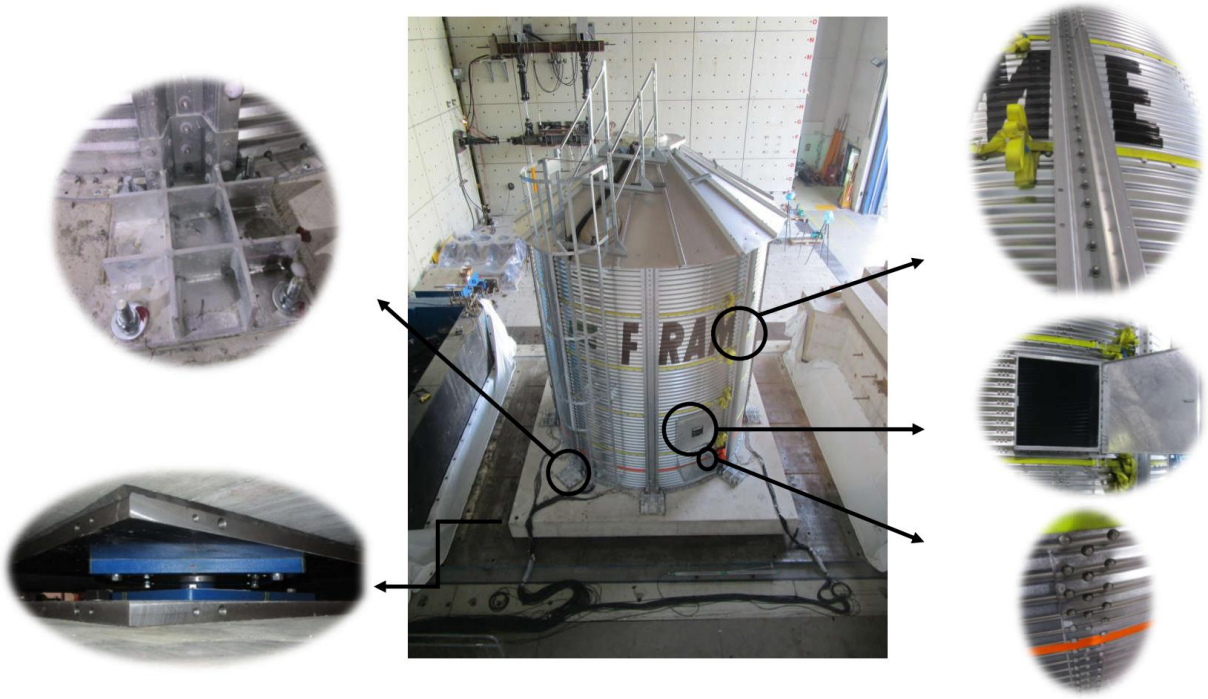

Figure 1: Global configuration of the base-isolated structural system

2.2 Isolation devices

Among the available technologies for seismic isolation, sliding devices have been chosen as the most suitable for the structural system under investigation. More specifically, Curved Surface Slider isolators can provide large amount of dissipated energy during motion, with a certain level of recentering capability, and consequently low residual displacements can be achieved at the end of a seismic event. In addition, a single curved sliding surface has been considered, given the overall geometry of the inner slider and the required maximum displacement demand, which can be easily accommodated by a single surface, with reasonable sizes of the devices.

The implemented Single Curved Sliding Surface isolators (SCSS), located at the four corners of the reinforced concrete plate, at the base of the silo. In Figure 2 a section of the 3D rendering of the adopted devices is shown, together with all the internal components. It can be noted that the devices are equipped with two individual sliding pads: at the bottom side of the device such a pad is capable to allow a rotational hinge, in order to accommodate the eventual rotations induced by the flexural deformations of the plate; on the other hand the upper material associated

to the sliding translational motion of the isolator, and provides the dissipative hysteretic frictional response. Both the sliding pad is made up of the Maurer Sliding Material MSM®: such material provides optimized frictional characteristics, in order to better control the seismic response of the system.

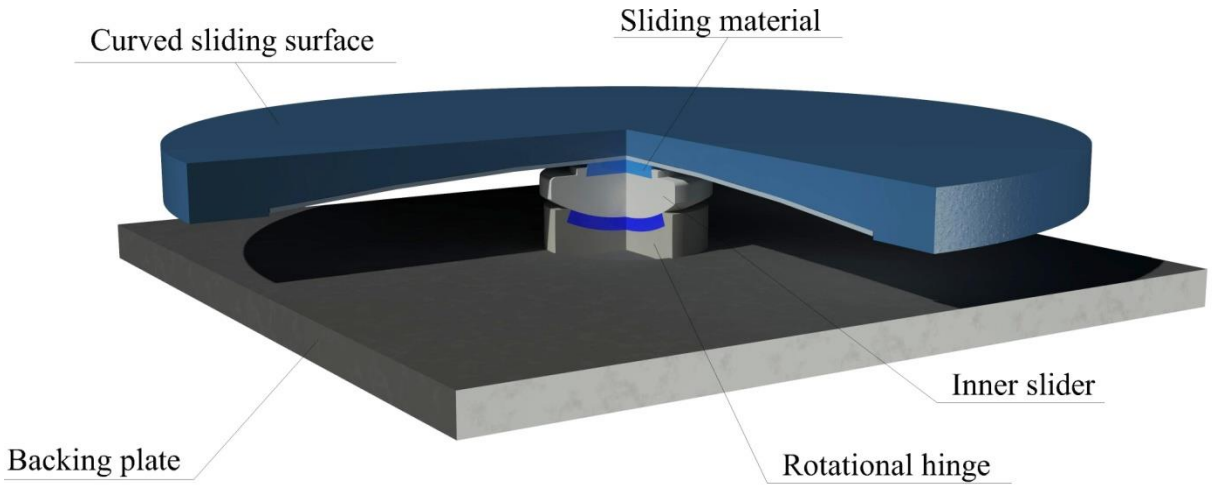

Figure 2: Internal section of the adopted devices.

The isolators have been designed and manufactured by the MAURER company (Germany) in order to obtain a period of 3 s (radius = 2.2364 m, max allowable displacement = 0.2 m) for the isolated-base silo. More specifically, the Maximum Credible Earthquake (MCE) seismic hazard level has been considered, represented by the response spectrum provided by Eurocode 8, Type 1 and Soil Class C, with a Peak Ground Acceleration (PGA) of 0,45g. Concerning the mechanical properties, 5% friction coefficient has been assumed, as the lower bound of the frictional properties under cyclic excitations, for a safe evaluation of the maximum displacement, which results equal to 200mm; finally, the equivalent radius of curvature of the device has been obtained, by assuming a mechanical vibration period of the system of 3.0sec, which corresponds to R_{eq} equal to 2,2346m. The devices have been installed with an ad hoc procedure, in order to avoid possible inclinations between the lower and the upper plates of all isolators, which are likely to lead to unexpected behaviors for the isolated-base structural system. In detail, once the devices have been installed on the shaking-table, a perfectly horizontal position for the r.c. plate has been set, and a very thin free space has been left between the plate itself and all the top steel plates of the isolators. Finally, mortar has been cast to fill the free space and to guarantee the proper setup.

2.3 Testing instrumentation

The tested silo specimen was intensively equipped with a number of sensors [11], as shown in Figure 3, including:

1- 4 load cells, positioned along the input direction, subdivided on 2 levels on both sides of the internal wall;

2- 18 uniaxial accelerometers, placed on different points of the shaking table, the r.c. base and different elevations of the silo external side of the wall and roof where oriented along the input direction (except for 2 accelerometers on the r.c. plate perpendicular to the input direction);

3- 6 triaxial accelerometers, randomly oriented within the granular solid, subdivided as: a- 4 over the height of the canter and b- 2 close to Stiffener #8;

4- 2 LVDTs, placed along both the input direction and the perpendicular one, to measure the displacement between the r.c. plate and the shaking table.

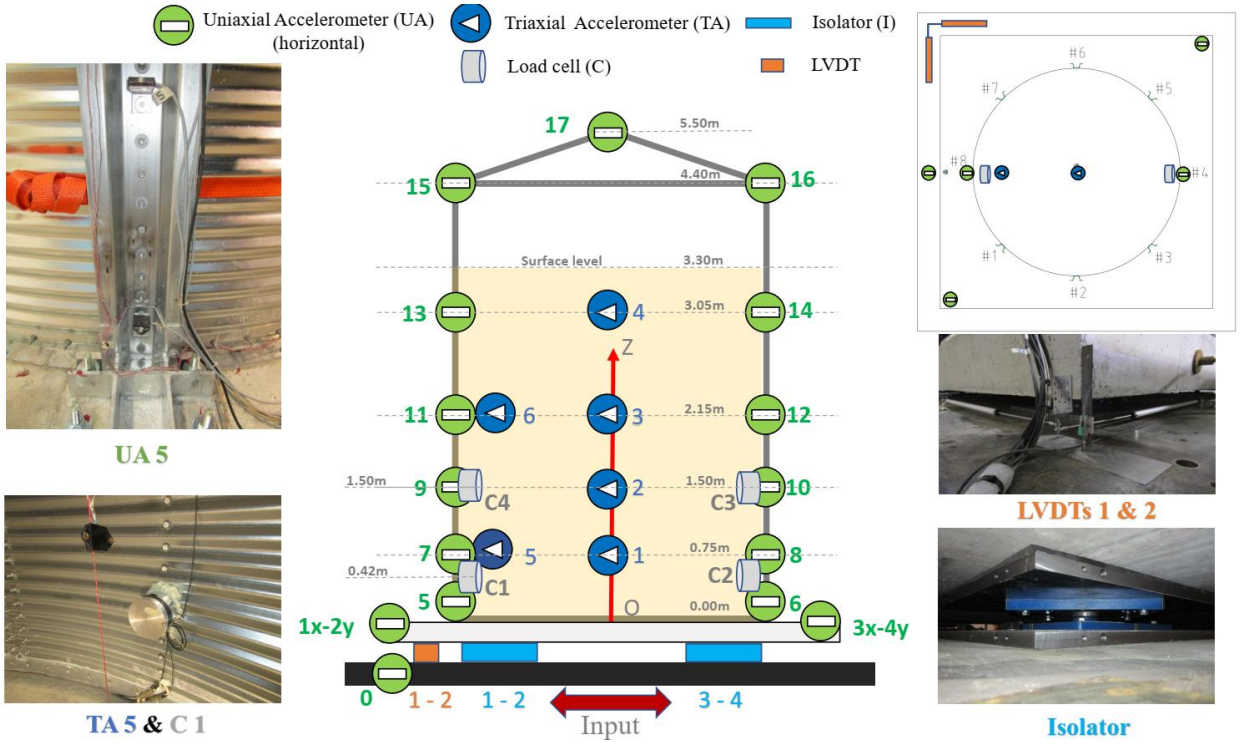

Figure 3: Structural monitoring sensors system of the silo.

3 TESTING PROTOCOL

Over 250 dynamic tests have been performed considering various inputs at the shaking table level. In this research work the outcomes of all the dynamic tests performed on the base-isolated configuration are presented and analyzed, by considering both earthquake and harmonic motions. More specifically, three ground acceleration time series have been selected as input signals for the shaking table: one signal has been artificially defined (a1), whereas the second (rs1) and the third (rs3) signal are represented by real natural recorded earthquakes, namely Campano Lucano earthquake (Irpinia, Italy, 23/11/1980) and Kalamata earthquake (Greece, 13/09/1986). Such seismic events have been chosen as input signals with "far-from-resonance" and "close-to-resonance" frequency content for the fixed-base silo, respectively. Furthermore, sinusoidal tests at constant amplitude and increasing frequency have been carried out to investigate the differences in silo response between the two tested configurations. Table 2 lists summarized the input types, the acceleration inputs and the frequency content of the isolated configuration tests.

Table 2: Testing protocol.

Signal Name	PGA [g]	Freq. [Hz]
random	0.05 - 0.20 - 0.30	-
a1 eqke	0.10 - 0.20 - 0.30 - 0.40 - 0.45 - 0.50	-
rs3 eqke	0.10 - 0.20 - 0.30 - 0.40 - 0.45 - 0.50	-
rs1 eqke	0.10 - 0.20 - 0.25 - 0.30 - 0.35	-
Pulse	0.10 – 0.20 – 0.30	
Harmonic (sinusoidal)	0.10 - 0.10	0.70 - 0.60

All reference signals for experimental earthquake simulations have been gradually scaled, according to the aforementioned scaling factors. In Figure 4 the response spectra of the adopted records, scaled at their maximum amplitudes of the testing protocol are shown.

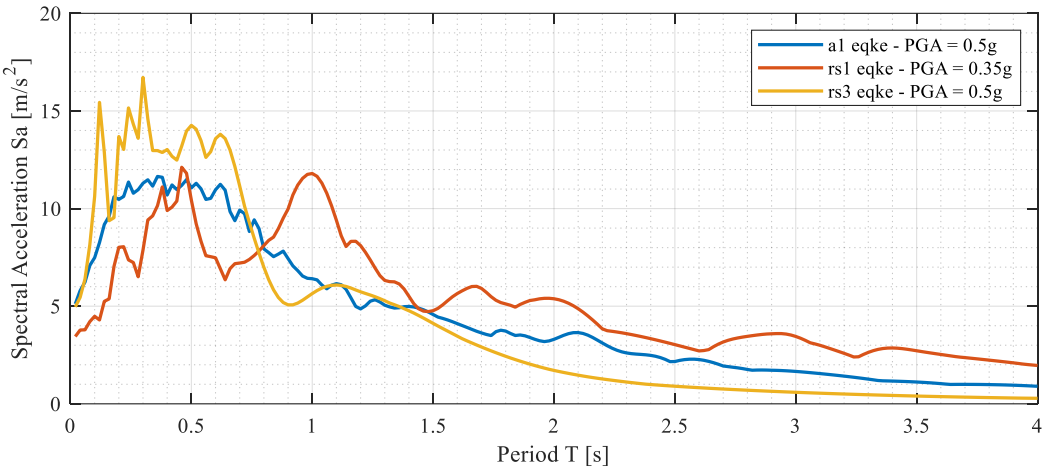

Figure 4: Response spectra of the adopted signals at maximum scale factors.

In addition, harmonic excitations have been applied at the shake table, in terms of multi-cycle sinusoidal time series of acceleration, in order to simulate what generally happens in characterization tests for isolation devices by means of testing equipment for seismic devices, as ruled by the European Standard code UNI: EN15129:2009 ([77]).
Table 3 introduces chronologically the complete testing program, including both the fixed-base and the isolated-base configurations.

Table 3: Complete testing program.

Fixed-Base Configuration			Isolated-Base Configuration		
Peak Table Acceleration	Test N.	Type of Signal	**Peak Table Acceleration**	Test N.	Type of Signal
0.07 g	1	random	**0.05 g**	148-165	random
0.10 g	2-9	sin 0.5 Hz	**0.10 g**	166-168	a1 eqke
	10-13	rs1 eqke	**0.30 g**	169-170	random
	14-16	a1 eqke	**0.10 g**	171-174	a1 eqke
	17-19	rs3 eqke	**0.20 g**	175-179	a1 eqke
0.15 g	20-21	random	**0.15 g**	180-182	random
0.20 g	22-26	sin 1 Hz	**0.30 g**	183-187	a1 eqke
	29-31	rs1 eqke	**0.20 g**	188	random
	32-34	a1 eqke	**0.40 g**	189-193	a1 eqke
	35-38	rs3 eqke	**0.45 g**	194	a1 eqke
	39-40	random	**0.50 g**	195	a1 eqke
0.30 g	41-45	sin 1 Hz	**0.55 g**	196	a1 eqke
	46-48	rs1 eqke	**0.20 g**	198-200	random
	49-51	a1 eqke	**0.10 g**	201-205	rs3 eqke
	53-55	rs3 eqke	**0.20 g**	206-210	rs3 eqke
0.40 g	56-59	sin 1 Hz	**0.30 g**	211-215	rs3 eqke
	60-62	rs1 eqke	**0.40 g**	216-220	rs3 eqke
	63-66	a1 eqke	**0.45 g**	221	rs3 eqke
	67-69	rs3 eqke	**0.50 g**	222	rs3 eqke
0.50 g	71-76	sin 1 Hz	**0.55 g**	223	rs3 eqke
	77-80	rs1 eqke	**0.10 g**	224-227	rs1 eqke
	81-83	a1 eqke	**0.20 g**	228-232	rs1 eqke
	84-86	rs3 eqke	**0.25 g**	233	rs1 eqke
0.07 g	88-89	random	**0.30 g**	234-235	rs1 eqke
0.15 g	90-91	random	**0.35 g**	236	rs1 eqke
0.20 g	92-93	random	**0.10 g**	238-242	pulse
0.25 g	94-96	random	**0.20 g**	243-247	pulse
0.10 g	97-101	sin 0.5 Hz	**0.30 g**	248	pulse
0.20 g	102-106	sin 1 Hz	**0.10 g**	249-253	sin 0.7 Hz
0.30 g	107-111	sin 1 Hz		254-256	sin 0.6 Hz
0.40 g	112-116	sin 1 Hz			
0.50 g	117-121	sin 1 Hz			
0.60 g	122	rs3 eqke			
	123	rs1 eqke			
	124	rs3 eqke			
	125	a1 eqke			
0.10 g	126-129	sin 5 Hz			
	130-134	sin 6 Hz			
	135-139	sin 7 Hz			
	140-145	sin 8 Hz			

4 MAIN RESULTS ON THE DYNAMIC RESPONSE OF THE FILLED SILO SYSTEM IN FIXED-BASE CONFIGURATION

Starting from the careful understanding of the reported historical data in the literature, the aforementioned large systematic experimental campaign has been planned and executed as a part of long term theoretical-experimental research at the EUCENTRE laboratory in Pavia (Italy), performing different series of shaking table tests on a full-scale ground-supported steel silo filled with soft wheat [11] in classical base boundary conditions (i.e., fixed-based configuration as commonly found in industrial facilities). The testing protocol of this first configuration was almost similar to the one presented in the previous chapter, except for the low frequency 1 Hz sinusoidal inputs used for other purposes different from those of the second configuration declared in this work. The main objective of that campaign was to investigate the actual response of a commercial silo specimen under different input types, either in terms of the principal dynamic properties, or the forces induced by the granular material onto the silo wall. The results showed that two ranges of damping ratio have been identified depending on the input acceleration magnitude: 5-10% when considering low magnitude input (0.05-0.1g) and 15-20% by introducing a relatively high acceleration input (accounting for the nature of the random input, and its different frequency contents). Such a difference in the response is strongly related to the physical nature of the granular solid (apparently, different than liquid), i.e., to the potential relative sliding mechanism between the granular layers which enhances the frictional dissipative behavior resulting in increasing damping with increasing acceleration. The filled silo system frequency was found to be around 11 Hz by introducing a random input type and using the classical analysis methods (see Chapter 5.2 of [11] for further details). On one hand, the measured frequency slightly diminished by increasing the input acceleration magnitude. On the other hand, granular compaction increased the stiffness of the stored material, resulting in increasing frequency. Finally, no noticeable dynamic amplification was captured between the response of the silo wall and the granular material at the corresponding height when introducing a sinusoidal input, while a growing amplification was noticed by increasing the acceleration magnitude of the real and artificial earthquake input up to 100% closer to the granular surface position.

5 PERFORMANCE OF THE ISOLATION SYSTEM

The silo has also been tested in seismically isolated conditions, by removing the steel connectors used to connect the r.c. plate to the table in the fixed-base configuration. Harmonic motions have been considered, for the calibration of the analytical model of the frictional properties of the isolation system, in order to simulate what is generally investigated through dynamic tests performed on a single device, in agreement with standard codes for anti-seismic devices; consequently the obtained frictional model can been used for numerical simulations, by adopting a simplified non-linear 2DOF system, and results have been compared to the experimental response returned by shaking table tests.

5.1 Experimental verification of the target frequency of the isolated system

The target mechanical frequency (0.3 Hz) of the isolated-base silo has been experimentally found from the spectrogram built with reference to the relative horizontal displacement (along the input direction) between the r.c. plate and the shaking-table during Test N. 196 (0.55g a1 earthquake), which is shown in **Figure 5**. More specifically, a the computation of the spectrogram of the analyzed signals provides a visual representation of its spectrum of frequencies as it varies with time, by considering a moving time window: such an analysis represents an extremely useful tool, which better highlights the largest frequency contents of a signals, which last longer within the whole duration of the simulation.

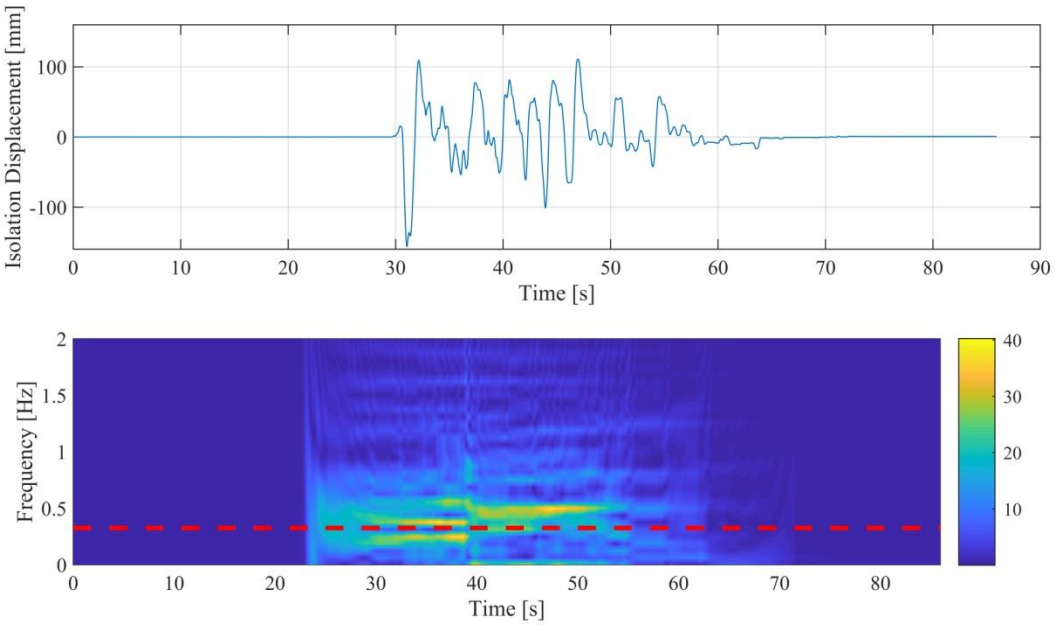

Figure 5: Spectrogram analysis of the isolation displacement time series.

In the common practice the dynamic experimental response of isolation devices is generally assessed through tests on single devices, according to the proper standard code (among the others, UNI: EN15129:2009 [77] and AASHTO 2014 [78],). Tests are carried out, by applying sinusoidal displacement signals with multiple cycles, and the force response is measured, in order to return the characteristic force-displacement hysteretic loops of the devices.

In this project, the dynamic properties of the overall isolation system have been evaluated, through actual shaking-table tests of the isolated configuration. Precisely, aiming at obtaining sinusoidal motions relatively between the shaking-table and the r.c. plate (namely the isolation displacement, as measured by the LVDTs), harmonic acceleration signals have been applied to the shaking-table. In the isolated configuration, the actuation force directly corresponds to the isolation force response, thus directly related to the whole set of four installed devices. Consequently, what is generally done on the single devices has been obtained, through the application of sinusoidal acceleration input waveforms at the base of the isolated silos, with a resulting sinusoidal-like displacement signal

has been obtained at the device level. Even though the effective displacement time series at the isolation devices does not correspond to a purely sinusoidal function, the frictional properties can be considered as path-independent for the adopted isolation technology, as reported in previous research work [82]. In Figure 6 the resulting hysteretic loops returned by Tests N. 253 and N. 256 are provided: the base shear force response has been normalized with respect to the total weight of the overall structural system, so that a preliminary analysis of the frictional properties can be noticed at zero displacement (i.e., no re-centering contribution).

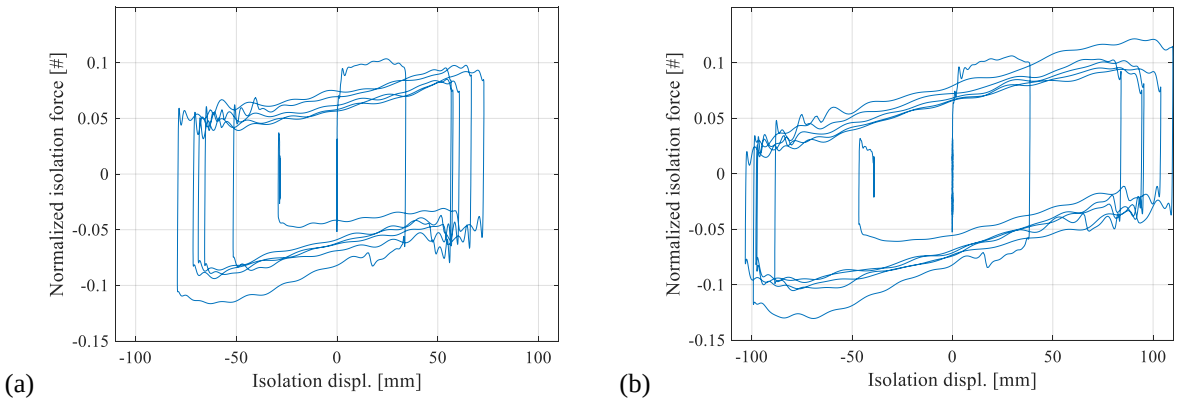

Figure 6: Experimental hysteretic loops of sinusoidal tests: (a) Test N. 253, (b) Test N. 256.

Graphical results show the commonly known cyclic effect of Curved Surface Slider devices: as the number of applied cycles increases, the frictional force response decreases, with consequent reduction of the hysteretic energy. Moreover, since an acceleration input signal has been applied at the shaking-table, the resulting isolation displacement time series for both tests do not have symmetric peak values of both amplitude and sliding velocity. Thus, in order to assess the frictional properties of the overall isolation system, the standard code UNI: EN15129:2009 has been applied, by considering the effective displacement and velocity demands for all cycles. The friction coefficient, can be computed, as a function of the experimental Energy Dissipated per Cycle (EDC) as follows:

$$\mu = \frac{EDC}{4 \cdot D_{max} \cdot W} \tag{1}$$

being D_{max} the mean value between the maximum and minimum displacement of the cycle, whereas W represents the vertical load applied to the device; in this case, since the force response is computed by considering the whole set of isolators, W represents the total weight of the system. Figure 7 presents the results in terms of peak displacement and velocity values for all cycles, together with a direct analysis of the cyclic effect, for both Tests N. 253 and N. 256.

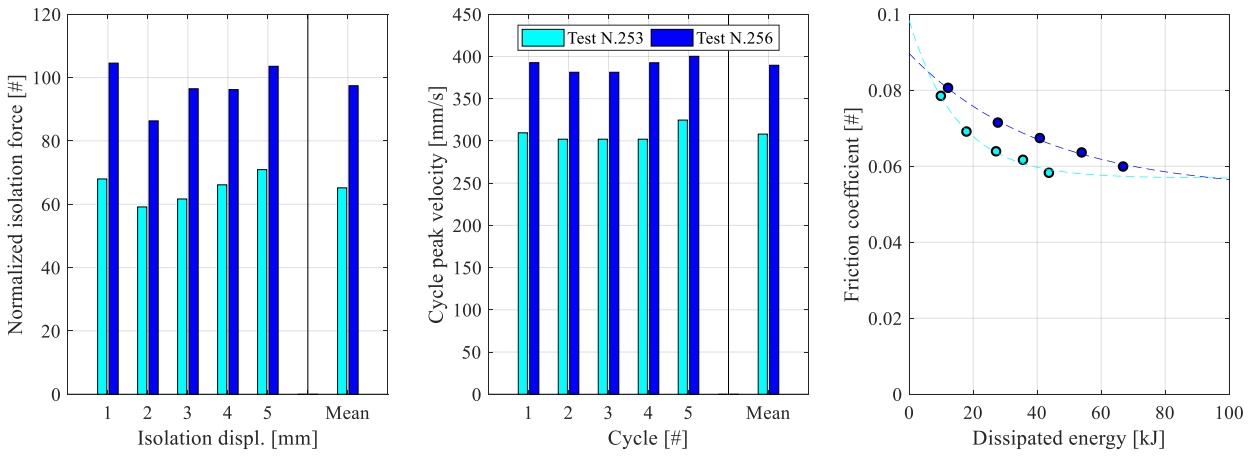

Figure 7: Dynamic properties of the isolation system (Test N. 253 and N. 256): (a) cycle peak displacement (b) cycle peak velocity (c) friction coefficient.

Experimental points have been used to obtain a best fit curve, characterized by the following expression:

$$\mu(t) = \mu_{VW} \cdot [(1-p) \cdot e^{-E(t)/E_o} + p] \tag{2}$$

which is able to describe the decay of the friction coefficient value with respect to the cumulative dissipated energy E(t) of the test [79]. Parameter μ represents the instantaneous value of friction coefficient, whereas μ_{VW} is the value associated to the applied vertical load and sliding velocity at the beginning of the motion; other important parameters are p, which is the asymptotic decay percentage for long-lasting input motions, and E_o which is the energy value which rules the decay trend of the curve. Since the decay curve is represented by an exponential equation, the parameter Eo always refers to the dissipated energy value which corresponds to 63% (actually $1 - e^{-1} \approx 0.63$) of the reduction of the variation between the initial and the asymptotic friction coefficient values (represented by μ_{VW} and $\mu_{VW} \cdot p$ respectively). In Table 4 numerical values of all parameters returned by the non-linear best-fit procedure are listed.

Table 4: Parameters of best-fit curves.

***f* [Hz]**	0.70	0.60
***μVW* [%]**	9.839	8.968
***Eo* [kJ]**	14.96	41.59
***p* [%]**	57.81	59.35

Results show similar starting frictional properties, corresponding to approximately 9.4% (average of the two values) of initial friction coefficient, as commonly happens when highly dynamic motions are applied to friction-based devices. Concerning the maximum decay associated to long-lasting input motions, same percentages have been found, even though individual values of sliding velocity have been considered. Interesting results have been found about parameter E_o, which highlight slightly different cyclic effects between the considered tests. Precisely in Test N. 253 a much faster decay of frictional properties has been experienced. This behavior is mainly due to the displacement amplitude, in comparison to the size of the sliding pad ([80]): in Test N. 253 a smaller displacement demand is averagely covered for all cycles (65mm, rather than 100mm for Test N. 256), and consequently more significant heating fluxes are originated at the sliding interface, which cause a faster decay of the friction coefficient. It has to be noted that what is commonly known as "cyclic effects" in sliding motions relates to the decreasing value of friction coefficient, as the applied movement keeps going, due to the heating flux which originates at all the implemented sliding surfaces. This behavior causes a decay of the frictional properties during the application of motion (i.e. during a seismic event), and the original value is restored as the motion stops and the sliding surfaces cool down. Thus, such a decay can not be considered as a wear of the sliding material, but it represents a special behavior of the lateral response of the considered isolation technology. Therefore, the choice of the numerical value of the friction coefficient to be assumed in the design phase deserve detailed assumptions, depending on the response parameters under consideration. As a general rule, safe approach are often applied: for the estimation of the displacement response, the lowest value of friction coefficient should be adopted, corresponding to the minimum asymptotic value under cyclic loading; on the other hand, in order to maximize the internal forces in the superstructure, the maximum value at the beginning of motion should be preferred.

5.2 Analytical model of the base-isolated system

Results of the harmonic tests have been used to calibrate an analytical model of the isolation system, in order to perform non-linear time history analyses of a simplified dynamic system, by applying the adopted ground motions of the experimental earthquake simulations. The overall system has been condensed to a lumped mass oscillator, with two degrees of freedom, and the isolation system has been properly modeled through a non-linear hysteretic behavior.

The overall structural system has been considered as a 2DOF oscillator, by adopting a linear elastic behavior for the silo, and a non-linear constitutive law for the isolation layer. In Figure 8 a scheme of the implemented dynamic system is shown.

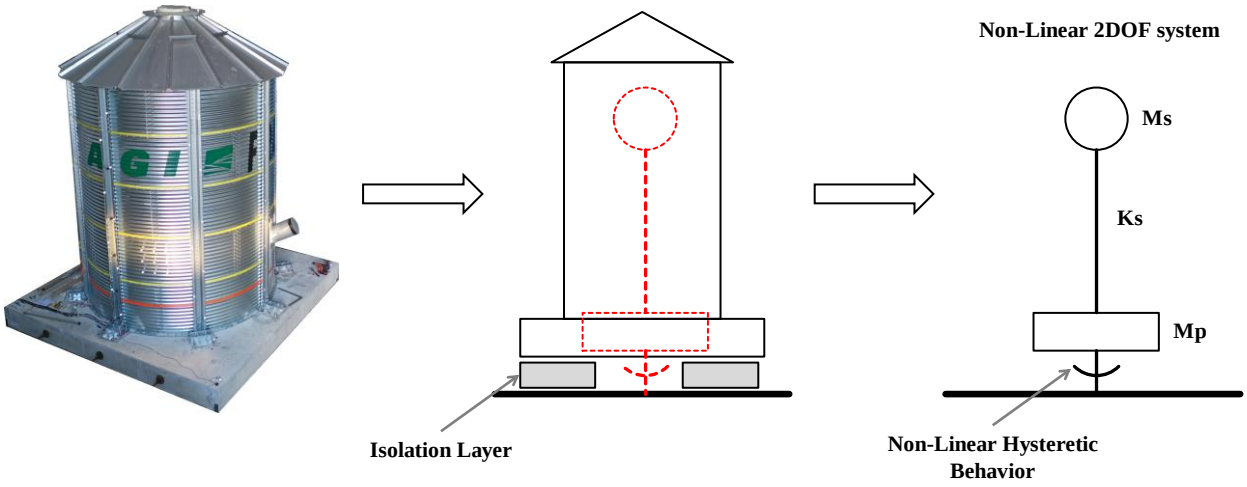

Figure 8: Condensed dynamic system of the structure.

At both the r.c. plate and the silo mass locations a single horizontal translational degree of freedom has been considered, and a global 2 degree of freedom system has been obtained. Thus, the system of dynamic equations can be obtained as follows.

$$\overline{\overline{M}} \cdot \begin{pmatrix} \ddot{u}_0 \\ \ddot{u}_1 \end{pmatrix} + \overline{\overline{K}} \cdot \begin{pmatrix} u_0 \\ u_1 \end{pmatrix} + \langle F_{is} \rangle \cdot \begin{pmatrix} 1 \\ 0 \end{pmatrix} = -\overline{\overline{M}} \cdot \begin{pmatrix} 1 \\ 1 \end{pmatrix} \cdot \ddot{x}_g \tag{3}$$

Given:

- $\overline{\overline{M}}$ the mass matrix of the simplified 2DOF system;
- $\overline{\overline{K}}$ the stiffness matrix of the simplified 2DOF system;
- u_i the considered translational degrees of freedom;
- $\ddot{x}_g$ the applied ground acceleration time series;
- $\langle F_{is} \rangle$ the isolation force response.

It is highlighted that the stiffness matrix is representative of the behavior of the silos only, whereas the force response of the isolation system is considered as a separate contribution, added to the first equilibrium equation.

In order to represent the most realistic force response of the isolation layer, a non-linear hysteretic rule has been implemented, in agreement to the following expression:

$$\langle F_{is} \rangle = W_{tot} \cdot \left(\frac{u_0}{R_{eq}} + k_c \cdot \mu(t) \cdot f_{NF} \right) \tag{4}$$

Being:

- W_{tot} the total structural weight of the system;
- R_{eq} the equivalent radius of curvature of the device;

- u_0 the translational degree of freedom at the center of mass location of the concrete slab (isolation level);
- $\mu(t)$ the stepwise changing friction coefficient;
- f_{NF} a normalized frictional hysteretic parameter;
- k_c a variation scale factor of the friction coefficient which rules the cyclic effect.

The hysteretic parameter f_{NF} has been adopted, by assuming an elasto-plastic rule, and has been related to the frictional behavior of the device (Figure 9), by considering a yielding displacement of 1,5mm.

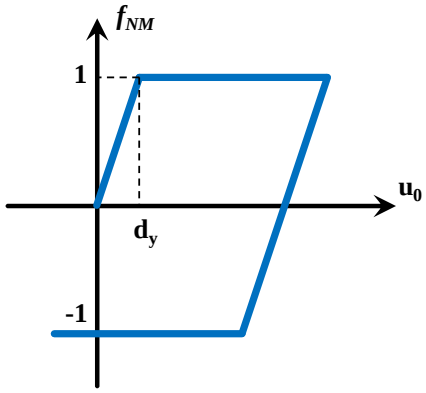

Figure 9: Bi-linear hysteretic parameter.

Such a parameter multiplies the friction coefficient at a given time instant, which is actually a function of time and varies step-by-step, depending on the cumulative dissipated energy, which is computed at each time step; the adopted function is represented by the calibration equation which has been computed by analyzing the outcomes of harmonic motions.

$$\mu(t) = \mu_{VW} \cdot \left[(1-p) \cdot e^{-E(t)/E_o} + p\right] \tag{5}$$

Thus, a numerical simulation of the harmonic tests has been computed, by adopting the analytical model, in order to check the accuracy of the representation of the isolation force response; in Figure 10 graphical results are shown.

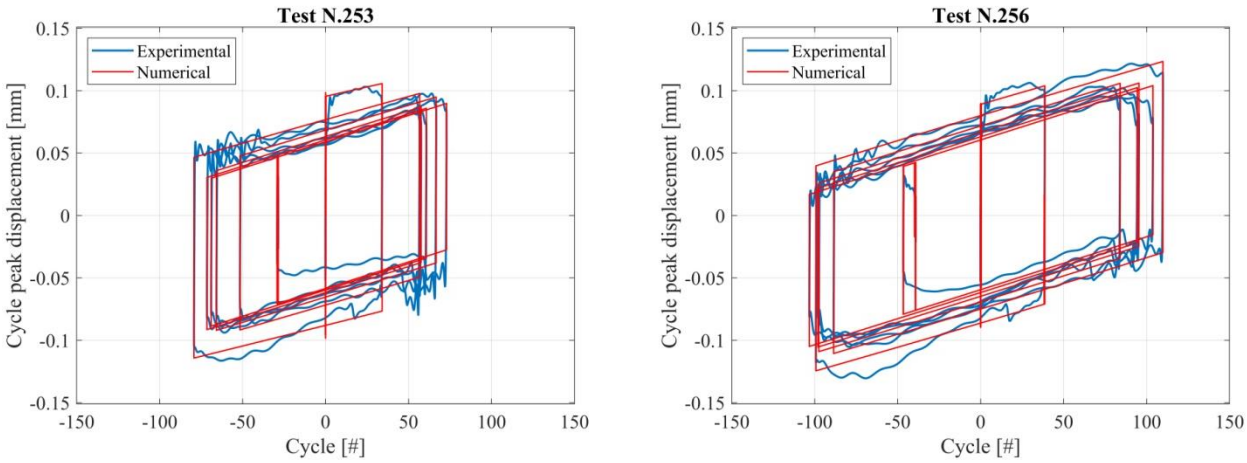

Figure 10: Calibrated numerical model for Test N. 253 (left) and N. 256 (right).

As can be noticed, the overall hysteretic behavior and the frictional decay of the isolation system can be fairly captured by the implemented numerical model, which then can be used for earthquake simulations through Non-Linear Time History Analyses. For all the analyses, the decay curve related to test N. 256 has been considered, since the motion is characterized by a number of cycles at large displacement amplitude, together with high values of sliding velocity, with a consequent moderate decay of frictional properties: such a behavior has been noticed also for earthquake tests, thanks to the analysis of the hysteretic response.

5.3 Comparison between experimental and numerical simulations

In this section the results of numerical simulations are presented, in comparison to the experimental response of a number of dynamic shaking table tests. More specifically, the aforementioned analytical model of the isolation system has been implemented within a non-linear two degrees of freedom oscillator, and Non-Linear Time History Analyses (NLTHA) have been performed, by considering the shaking table acceleration feedback signal as an input reference for the equivalent numerical system. In Figure 11 and Figure 12 results are reported in term of hysteretic and displacement responses for Sinusoidal and Pulse-like ground motions.

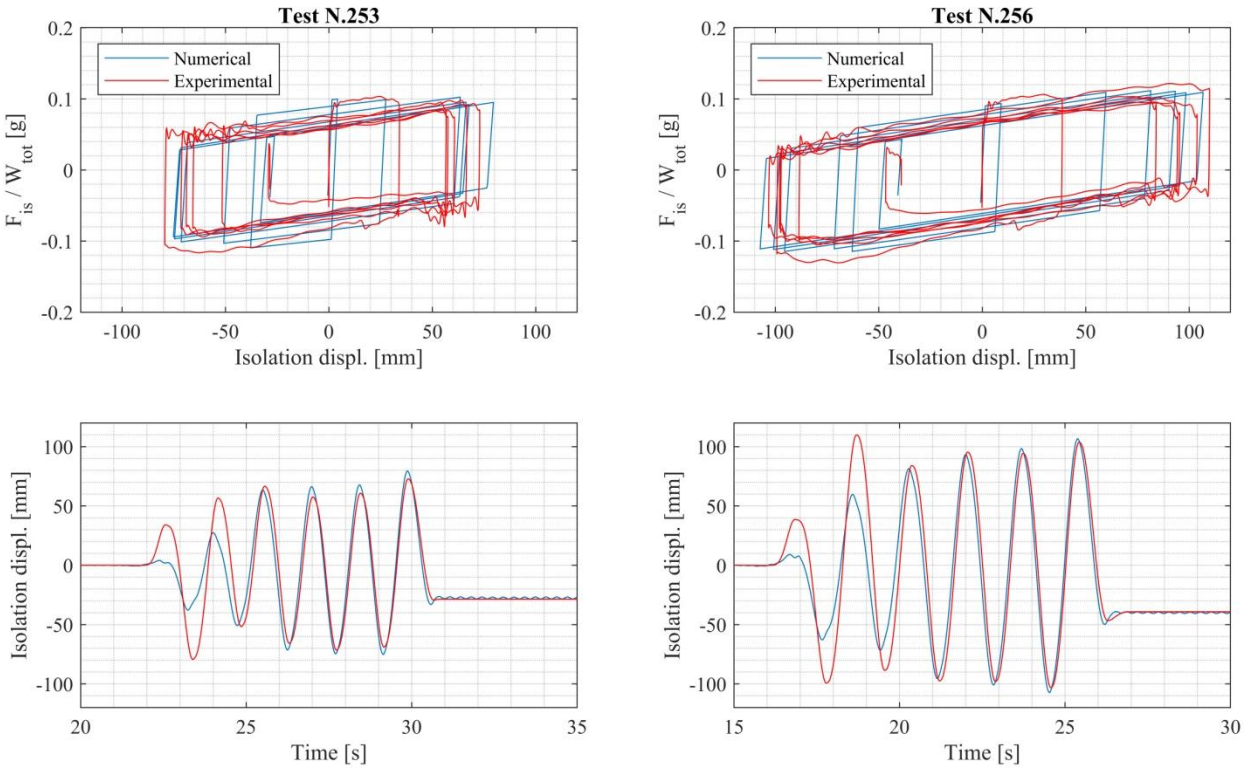

Figure 11: NLTHA simulations for Sinusoidal Test N. 253 (left) and N. 256 (right).

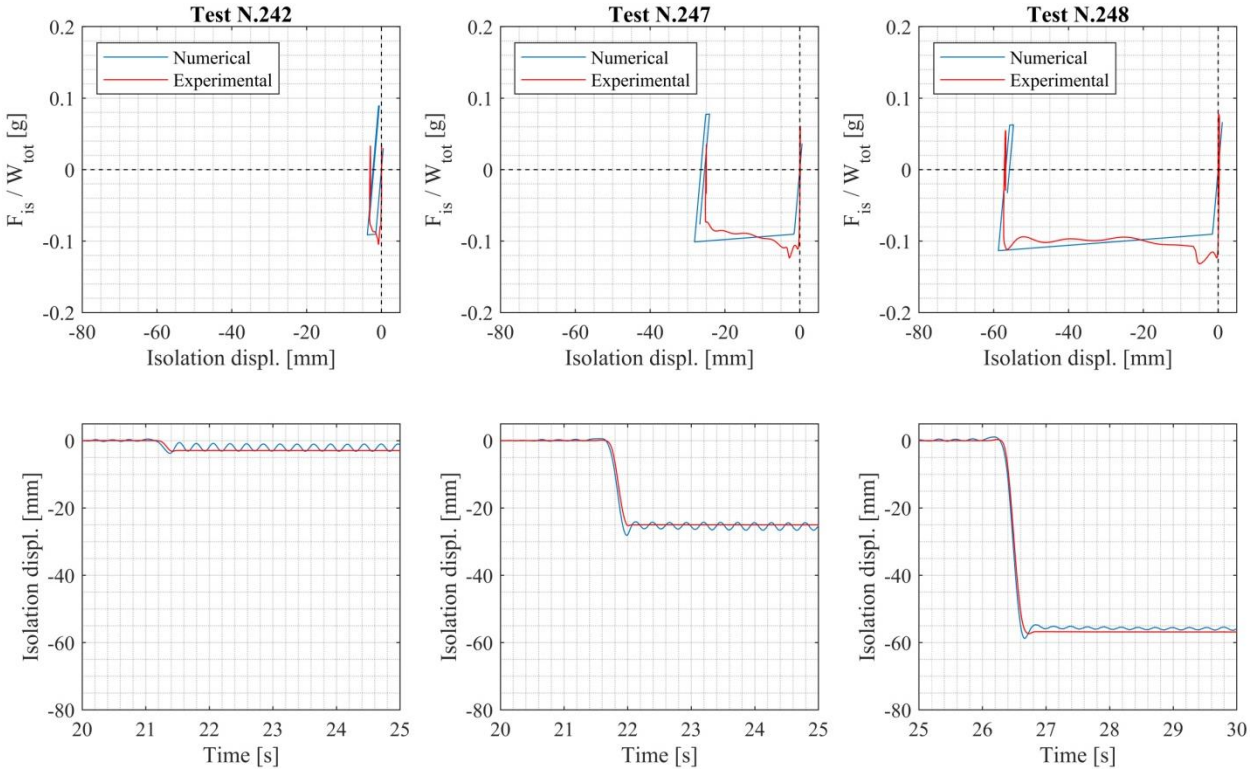

Figure 12: NLTHA simulations for Pulse-like Test N. 242 (left), 247 (center) and N. 248 (right).

In Figure 13 results of the numerical simulations have been directly compared to the outcomes of the correspondent experimental earthquake tests, by considering the adopted ground motions scaled at maximum amplitude.

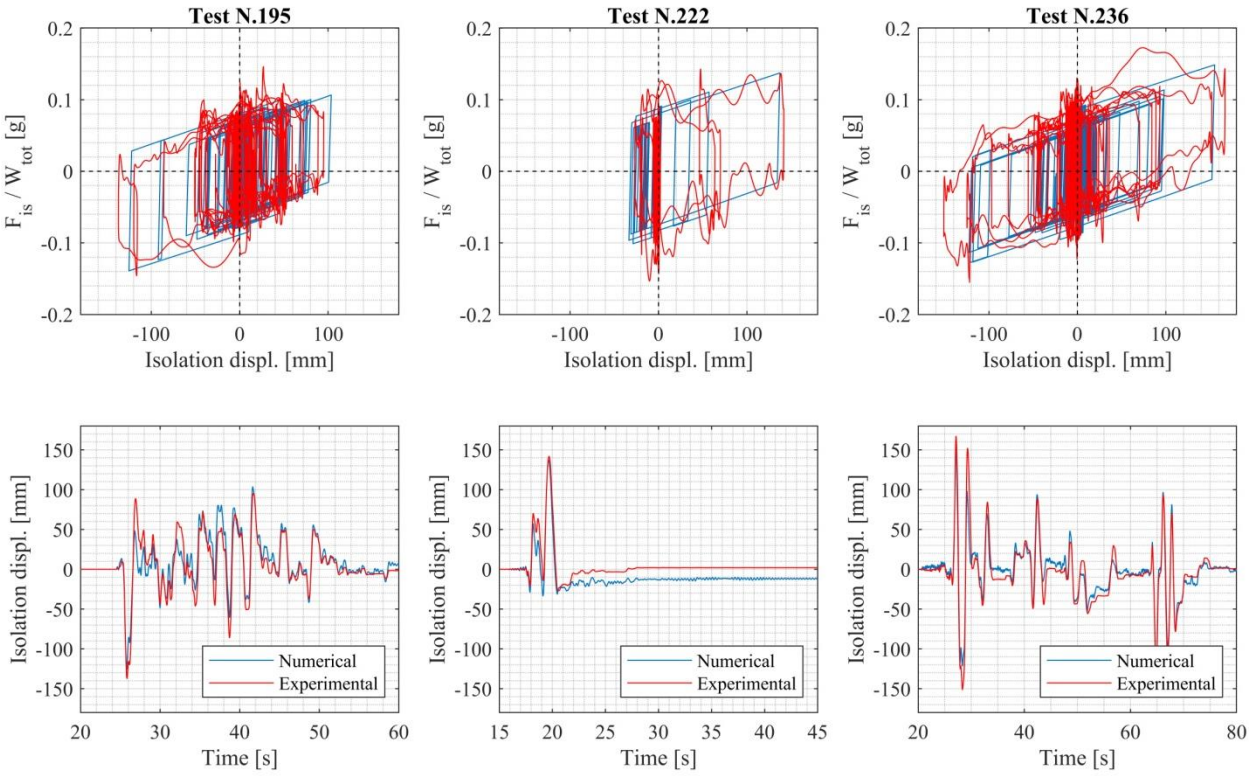

Figure 13: NLTHA simulations for Test N. 195 (*a1* - left), N. 222 (*rs3* - center) and N. 236 (*rs1* - right).

Results are presented in terms of force-displacement hysteretic response and isolation displacement time series. It can be noted that the overall behavior is averagely captured by the simplified numerical model of the system, even though a certain discrepancy can be detected, in terms of difference between the peak displacement demands. More specifically, the variation percentage between the numerical and the experimental peak displacements at the isolation level are –8.67%, –3.20% and –7.12% respectively for records ***a1***, ***rs3*** and ***rs1***. As a general comment, the numerical prediction of the peak displacement demand of the isolation layer is slightly underestimated, in comparison to the experimental response, even though variations lower than 10% can be detected, and a fairly good representation of the frictional decay behavior is obtained.

6 DYNAMIC RESPONSE OF THE FILLED SILO SYSTEM IN ISOLATED-BASE CONFIGURATION

This chapter provides an insight into the response of the isolated filled silo system in terms of the differences between the acceleration measured at the base of the silo and the input one at the shaking table level, the peak acceleration profiles along the silo height and the dynamic overpressures (i.e., the additional pressures provoked by

the dynamic input with respect to the static pressures) as measured from the load cells. The efficiency of the isolation system and the benefits offered by the isolated-base configuration with respect to the fixed-base configuration are presented and discussed in qualitative and quantitative ways.

6.1 Peak shaking table accelerations vs. peak silo base accelerations

The four Curved Surface Sliders guaranteed the reduction of the peak acceleration felt by the superstructure (i.e., the filled silo system). Figure 14 reports the time history registrations of the accelerations and their counterpart in the frequency domain (FFT output: amplitude spectrum) induced by the artificial and real earthquakes (a1, rs1 and rs3), in which the peak values measured on the shaking table and on the r.c. plate are highlighted. For instance, in Test 223, with a nominal peak acceleration magnitude of 0.55 g, the peak table acceleration reached a value of 0.61 g, while the maximum acceleration felt by the silo base didn't exceed 0.14 g, thus providing a decrement of more than 75%. Table 5 provides a summary of the isolation system efficiency in terms of peak acceleration differences between the two aforementioned levels. It should be clarified that random input tests showed different trending than the other types of inputs, which can be understood in the light of the wide frequency content of the signal, also approaching the system frequency and thus triggering resonance phenomena. Moreover, artificial earthquake with a very low acceleration magnitude (0.065 g) as well as pulse input with a similar magnitude showed a similar behavior. That is mainly associated to the fact that the isolators were not activated by the small intensity, as it will be discussed later. Finally, in Figures 14b, 14d and 14e, the response reduction provided by the isolation system from the shaking table level to the silo base level can be also clearly recognized in the frequency domain (in terms of amplitude spectra) for frequencies higher than the fundamental one of the base-isolated silo (around 0.3 Hz).

(a)

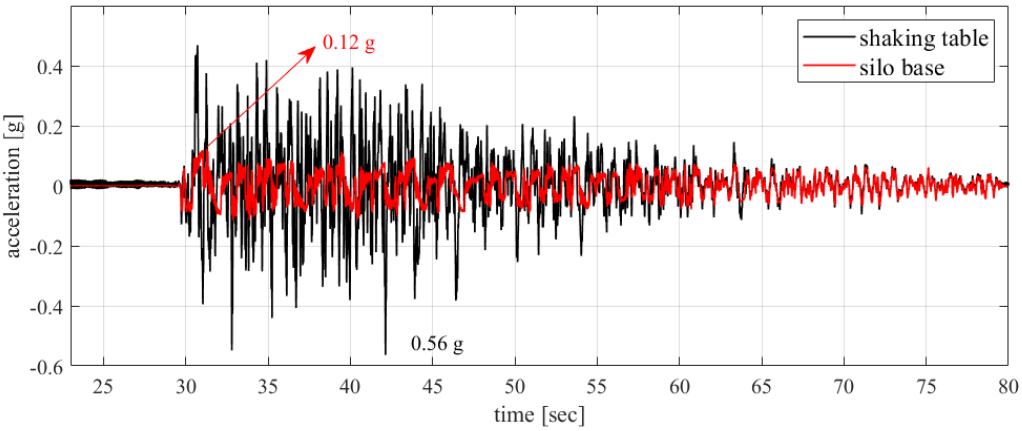
shaking table
silo base
0.12 g
0.56 g
acceleration [g]
time [sec]

(b)

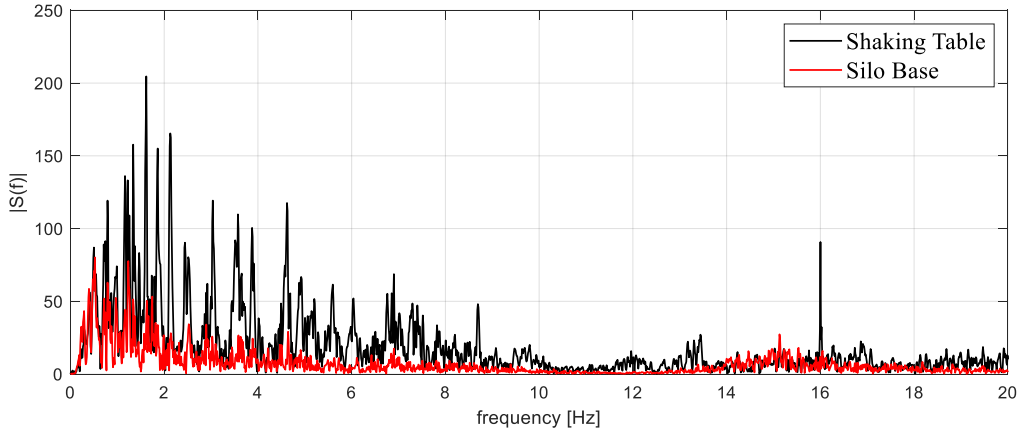
Shaking Table
Silo Base
|S(f)|
frequency [Hz]

(c)

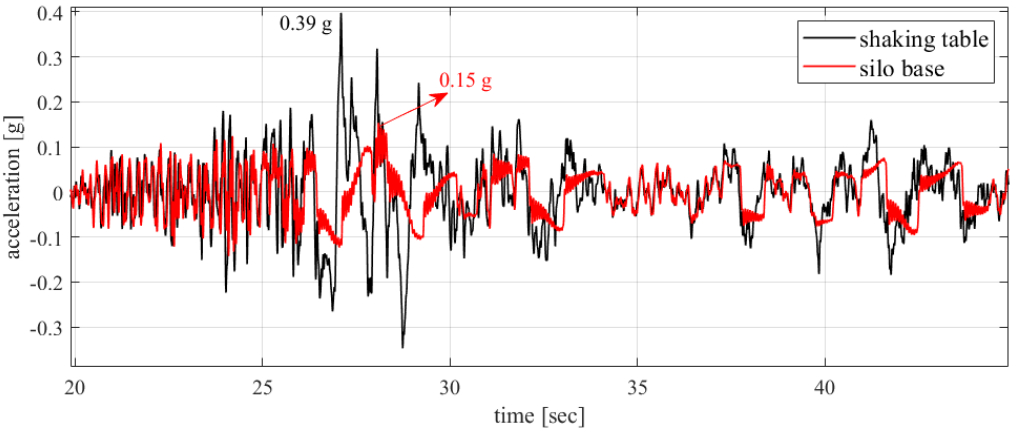
shaking table
silo base
0.39 g
0.15 g
acceleration [g]
time [sec]

(d)

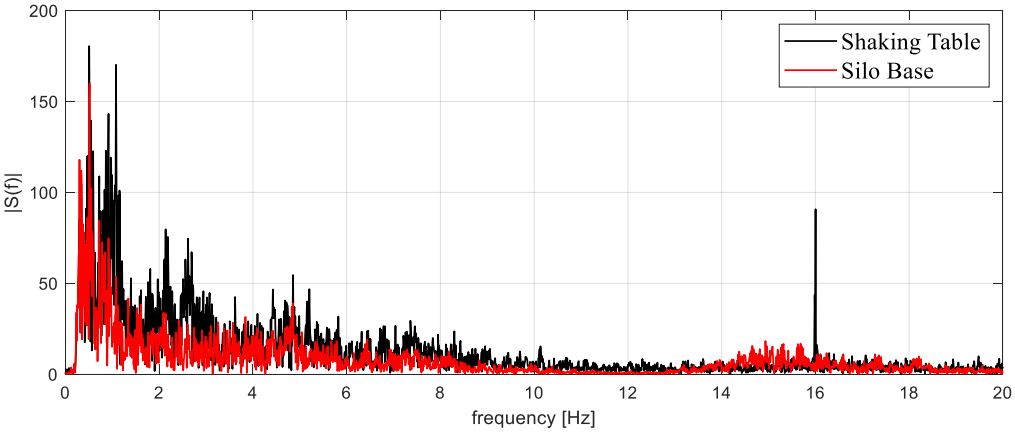

(e)

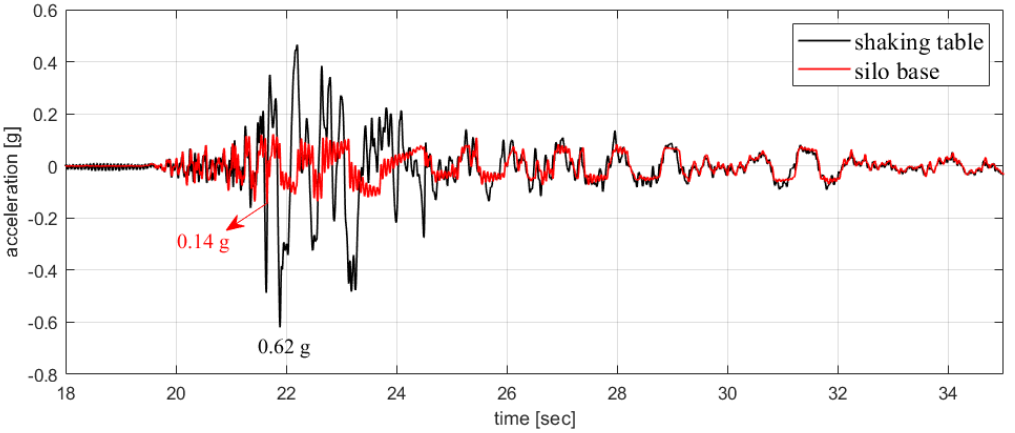

(f)

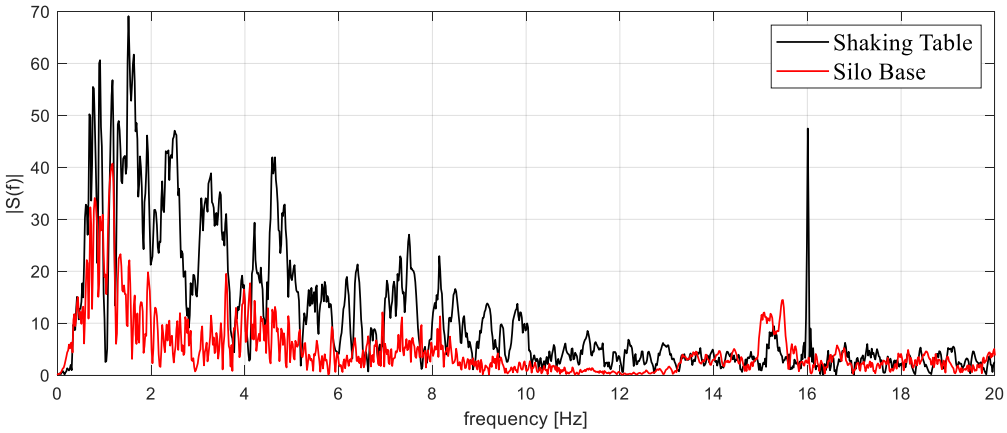

Figure 14: Time history registration and FFT output of: a- & b-Test 196 (a1) and c- & d-Test 236 (rs1) and e- & f- Test 223 (rs3), measured from both shaking table and isolated-base.

Table 5: Isolation effect on the peak acceleration from both shaking table and silo base levels.

Test	Input	Shaking table acc.	Silo base acc.	Difference	Test	Input	Shaking table acc.	Silo base acc.	Difference
[-]	[-]	[g]	[g]	[%]	**[-]**	[-]	[-]	[-]	[%]
146	random	0.024	0.029	21%	**202**	rs3 eqke	0.107	0.086	-19%
147	random	0.033	0.030	-9%	**203**	rs3 eqke	0.118	0.093	-21%
148	random	0.074	0.092	24%	**204**	rs3 eqke	0.119	0.094	-21%
149	random	0.070	0.130	84%	**205**	rs3 eqke	0.101	0.097	-4%
150	random	0.074	0.104	40%	**206**	rs3 eqke	0.143	0.104	-27%
151	random	0.050	0.041	-18%	**207**	rs3 eqke	0.228	0.134	-41%
152	random	0.045	0.038	-14%	**208**	rs3 eqke	0.179	0.145	-19%
153	random	0.079	0.081	3%	**209**	rs3 eqke	0.197	0.148	-25%
154	random	0.060	0.055	-9%	**210**	rs3 eqke	0.215	0.144	-33%
155	random	0.056	0.068	22%	**211**	rs3 eqke	0.177	0.140	-21%
156	random	0.064	0.098	52%	**212**	rs3 eqke	0.320	0.140	-56%
157	random	0.071	0.095	35%	**213**	rs3 eqke	0.287	0.133	-54%
158	random	0.064	0.112	76%	**214**	rs3 eqke	0.306	0.136	-56%
159	random	0.078	0.094	21%	**215**	rs3 eqke	0.321	0.130	-60%
160	random	0.090	0.121	35%	**216**	rs3 eqke	0.304	0.146	-52%
161	random	0.091	0.137	51%	**217**	rs3 eqke	0.436	0.145	-67%
162	random	0.062	0.129	108%	**218**	rs3 eqke	0.419	0.134	-68%
163	random	0.074	0.092	24%	**219**	rs3 eqke	0.427	0.133	-69v
164	random	0.070	0.130	84%	**220**	rs3 eqke	0.401	0.121	-70%
165	random	0.074	0.104	40%	**221**	rs3 eqke	0.516	0.139	-73%
166	a1 eqke	0.075	0.069	-8%	**222**	rs3 eqke	0.545	0.126	-77%
167	a1 eqke	0.110	0.073	-33%	**223**	rs3 eqke	0.620	0.140	-77%
168	a1 eqke	0.153	0.093	-39%	**224**	rs1 eqke	0.070	0.059	-15%
169	random	0.164	0.182	11%	**225**	rs1 eqke	0.117	0.086	-26%
170	random	0.134	0.148	11%	**226**	rs1 eqke	0.105	0.090	-14%
171	a1 eqke	0.065	0.073	12%	**227**	rs1 eqke	0.111	0.089	-20%
172	a1 eqke	0.091	0.091	0	**228**	rs1 eqke	0.137	0.090	-35%
173	a1 eqke	0.115	0.088	-24%	**229**	rs1 eqke	0.192	0.102	-47%
174	a1 eqke	0.110	0.090	-18%	**230**	rs1 eqke	0.237	0.112	-53%
175	a1 eqke	0.139	0.094	-32%	**231**	rs1 eqke	0.203	0.115	-43%
176	a1 eqke	0.238	0.108	-55%	**232**	rs1 eqke	0.224	0.126	-44%
177	a1 eqke	0.236	0.115	-51%	**233**	rs1 eqke	0.268	0.135	-50%
178	a1 eqke	0.231	0.117	-49%	**234**	rs1 eqke	0.322	0.140	-56%
179	a1 eqke	0.208	0.122	-41%	**235**	rs1 eqke	0.362	0.139	-62%
180	random	0.206	0.258	26%	**236**	rs1 eqke	0.398	0.154	-61%
181	random	0.214	0.147	-31%	**237**	pulse	0.026	0.029	13%
182	random	0.224	0.205	-8%	**238**	pulse	0.045	0.046	3%
183	a1 eqke	0.154	0.102	-34%	**239**	pulse	0.065	0.071	9%
184	a1 eqke	0.233	0.125	-46%	**240**	pulse	0.102	0.076	-26%
185	a1 eqke	0.278	0.131	-53%	**241**	pulse	0.102	0.073	-28%
186	a1 eqke	0.298	0.125	-58%	**242**	pulse	0.104	0.073	-30%

187	a1 eqke	0.320	0.118	-63%	**243**	pulse	0.094	0.070	-25%
188	random	0.217	0.162	-25%	**244**	pulse	0.134	0.079	-41%
189	a1 eqke	0.220	0.104	-53%	**245**	pulse	0.174	0.088	-49%
190	a1 eqke	0.327	0.125	-62%	**246**	pulse	0.209	0.104	-50%
191	a1 eqke	0.404	0.118	-71%	**247**	pulse	0.193	0.090	-54%
192	a1 eqke	0.380	0.120	-68%	**248**	pulse	0.276	0.097	-65%
193	a1 eqke	0.393	0.128	-67%	**249**	sin 0.7 Hz	0.089	0.076	-15%
194	a1 eqke	0.461	0.133	-71%	**250**	sin 0.7 Hz	0.140	0.082	-41%
195	a1 eqke	0.516	0.133	-74%	**251**	sin 0.7 Hz	0.157	0.086	-45%
196	a1 eqke	0.563	0.123	-78%	**252**	sin 0.7 Hz	0.196	0.093	-53%
197	a1 eqke	0.029	0.029	-2%	**253**	sin 0.7 Hz	0.177	0.097	-45%
198	random	0.286	0.198	-31%	**254**	sin 0.6 Hz	0.113	0.074	-35%
199	random	0.205	0.132	-35%	**255**	sin 0.6 Hz	0.144	0.092	-36%
200	random	0.202	0.140	-31%	**256**	sin 0.6 Hz	0.182	0.107	-41%
201	rs3 eqke	0.085	0.073	-14%					

6.2 Peak acceleration profiles and reductions

In comparison to Figure 12 in [Silvestri et al., 2022], Figure 15 a and b provide acceleration profiles measured along the height of the silo wall, as well as along the height of the stored material in the center of the silo, as obtained for the pulse input (notice that, in the fixed-base configuration, 1 Hz sinusoidal inputs with different input magnitude were used). Both absolute and normalized (with respect to the silo base level) acceleration values are provided. First, it should be clearly highlighted that the shaking table peak acceleration diminished by 35% - 65% at the silo base level by means of the four isolators. Second, quite similarly to the results obtained with the 1 Hz sinusoidal input for the fixed-base configuration, the pulse input for the isolated-base configuration did not provoke any substantial amplification over the height of the monitored points with respect to the base level of the silo. However, an increment of the acceleration in the range of 5% - 35% was observed close to the granular surface level.

Figure 15 c and d provide the acceleration profiles as obtained for the close-to-resonance real earthquake inputs with increasing peak table acceleration. The results show higher efficiency of the isolators reflected in greater acceleration reductions between the shaking table and the isolated system, up to 77%. On one hand, the same qualitative and quantitative behavior was detected for all accelerometers placed between the base level and the granular surface, for earthquake input scaled at higher intensities (in the range 0.2 g – 0.6 g). On the other hand, some important amplifications were captured between the granular surface level and the silo roof top. The upper part of the steel silo might be seen as a secondary system vibrating above the top surface of the granular solid. The loose nature of the granular surface (with respect to the lower compacted layers) is a potential reason for such an amplification (from the results of the triaxial accelerometers), while the lack of containment provided by the granular solid in the upper level of silo might have caused the noticeable increasing acceleration values (similarly to what happened also for the fixed-based configuration). Sloshing effects are usually relevant for liquid tanks whilst they are not likely to happen for filled silo systems, due to the essential difference in the mechanical behavior of any frictionless liquid and any granular material like wheat. For instance, the mechanical behavior of wheat is governed by the internal friction coefficient which might be characterized by relatively large values (e.g., in the range of 0.5-

0.6). Finally, Test 205 which is characterized by a small peak table acceleration of around 0.1 g showed a quite different behavior. It might be affected by the lower-band limitation of the isolator functionality with low acceleration levels comparable to the friction coefficient of the sliding surface, leading to an almost vertical line between the shaking table and the silo base levels.

Figure 15 e and f provide the acceleration profiles as obtained for the sinusoidal inputs with decreasing frequency (the intention was to gradually approach the isolation frequency target, from 0.7 Hz toward 0.3 Hz but the tests were stopped at 0.6 Hz due to very large displacements) with constant 0.1 g peak table acceleration. A reduction of about 35% - 50% was observed between the shaking table and the silo base. The results do not show any noticeable amplification over the height (except for the loose granular surface level), differently from the fixed-base configuration where a maximum increment of the acceleration was detected of around 300% by approaching the filled silo frequency.

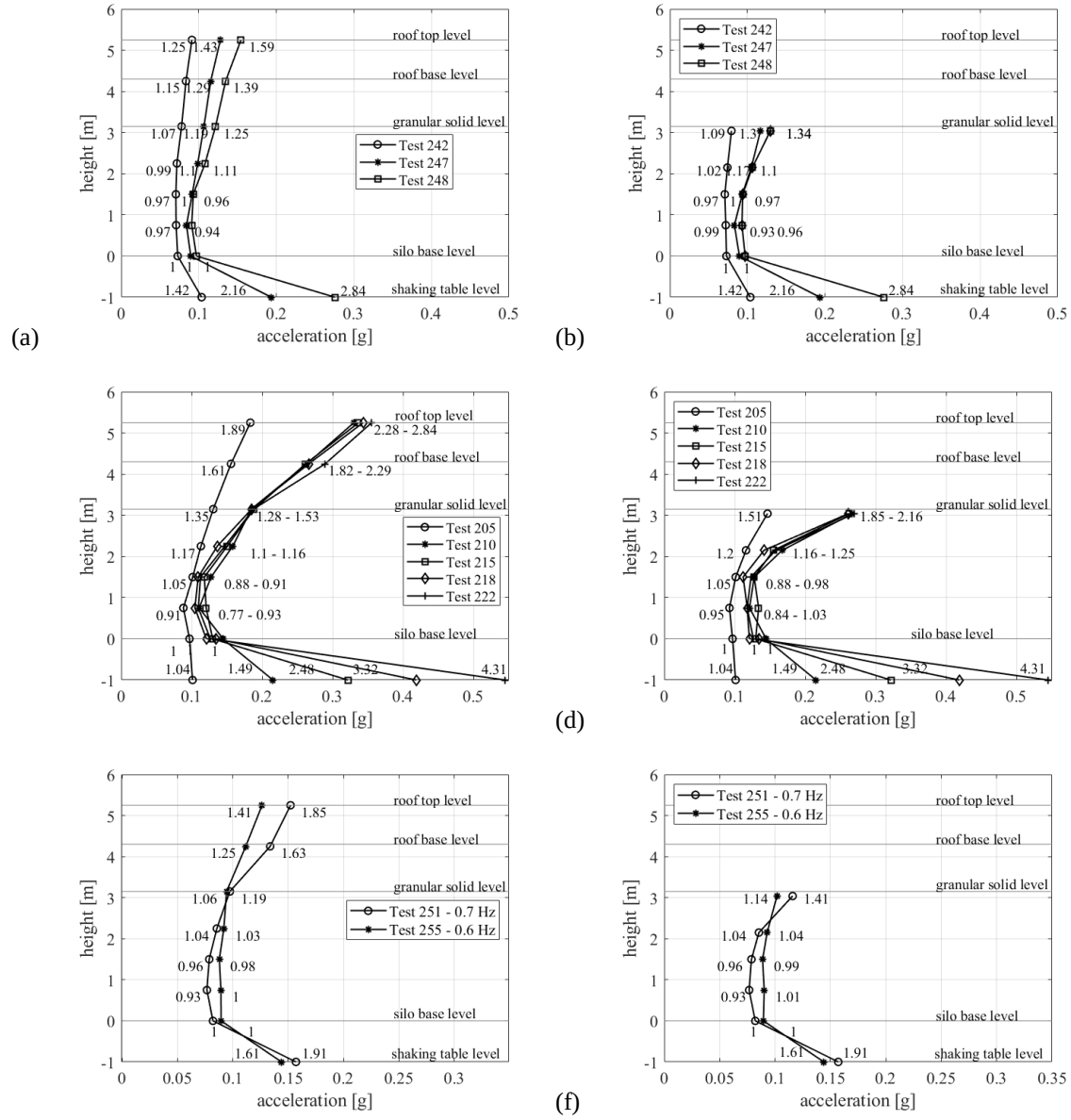

Figure 15: Vertical profiles of the peak horizontal accelerations and corresponding dynamic amplification factors; for pulse input: (a) along the silo wall and (b) inside the granular material in the middle section; rs3 earthquake input: (c) along the silo wall and (d) inside the granular material in the middle section; and for multi-frequency 0.1 g sinusoidal input: (e) along the silo wall and (f) inside the granular material in the middle section.

In more detail, a comparison is made between the behaviors of the fixed-based and the isolated-based configurations. Reference is made only to the case of real earthquake rs3, and Test 205 is neglected since the isolators were not actually active at its corresponding acceleration magnitude. The results of Tests 210, 215, 220 and 222 of the isolated-based configurations are compared with the results of Tests 86, 54, 69 and 86 of the fixed-based configuration, which mainly correspond in terms of peak table acceleration.

Figure 16 and Table 6 show that the isolation system was actually capable of mitigating the acceleration magnitudes in all monitored positions from the silo base up till the fifth monitored level (corresponding to 2.25 m, or where the wheat is effectively compacted), with a reduction in the range of 30% - 50% for PTA equal to 0.2g, and in the range of 55% - 85% for all other higher PTAs (0.3g, 0.4g and 0.5g). However, it can be noticed that the efficiency in terms of reduced measured accelerations is lower for the granular layers close to the surface level, where the reductions get dropped by 10%-15%. Finally, these reductions become even much lower at the roof base and top levels, where there was no supporting wheat from the internal side of the silo.

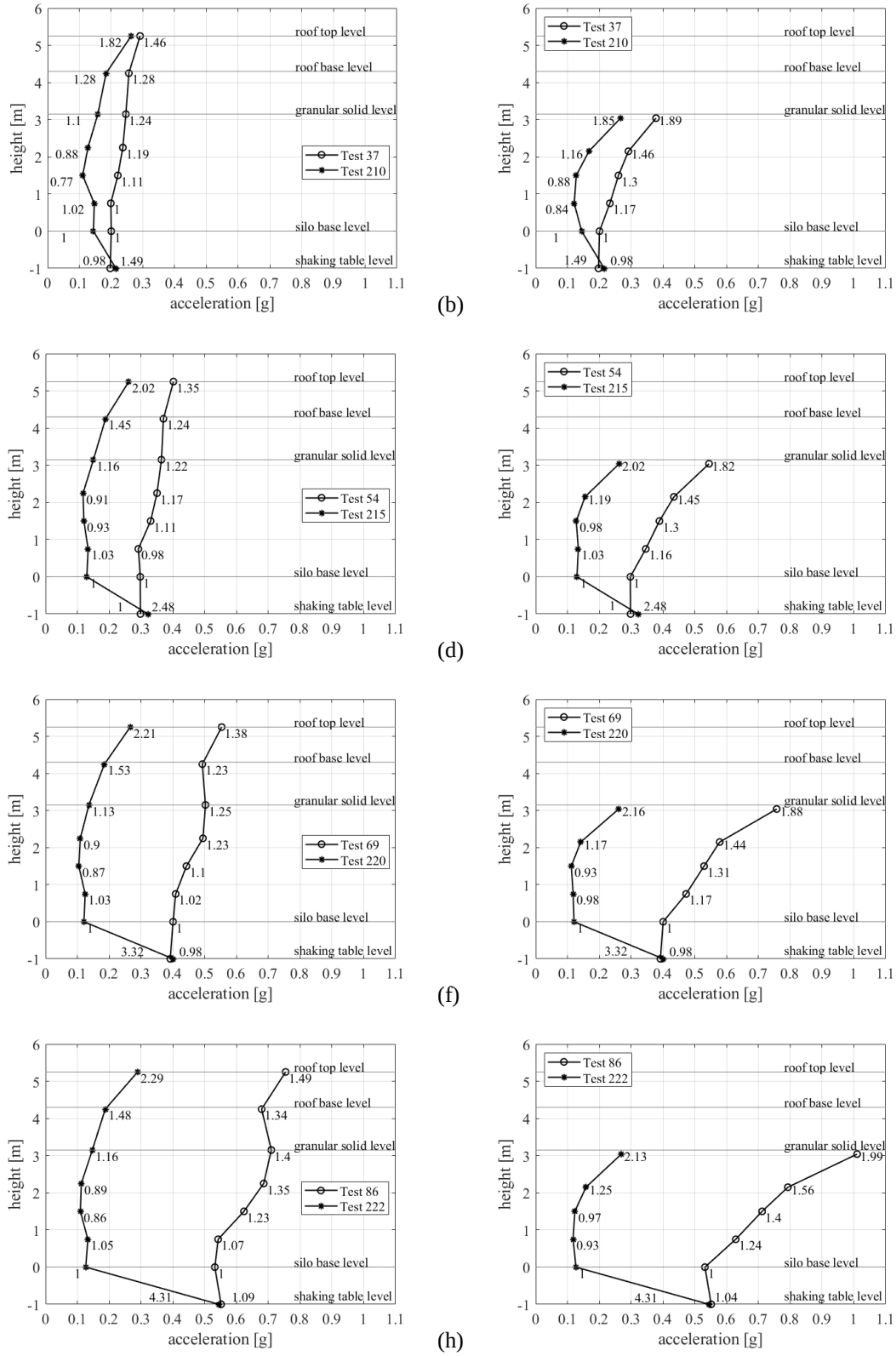

Figure 16: Vertical profiles of the peak horizontal accelerations and corresponding dynamic amplification factors between the fixed and isolated-base configurations in case of rs3 earthquake input: nominal PTA 0.2g,

0.3g, 0.4 g and 0.5g (a) (c) (e) (g) along the silo wall and (b) (d) (f) (h) inside the granular material in the middle section.

Table 6: Peak acceleration reductions from the monitored levels between the fixed and isolated-base configuration with real earthquake input rs3.

Test		37 /210		54/214		69/220		86/222	
Level / Vertical section		Wall	Internal	Wall	Internal	Wall	Internal	Wall	Internal
-0.40	shaking table level	-	-	-	-	-	-	-	-
0.00	silo base level	-34%	-34%	-60%	-60%	-70%	-70%	-75%	-76%
0.75	Internal level	-33%	-53%	-58%	-64%	-70%	-75%	-75%	-82%
1.50	Internal level	-54%	-55%	-66%	-70%	-77%	-79%	-82%	-83%
2.15	Internal level	-51%	-48%	-69%	-67%	-78%	-76%	-83%	-81%
3.05	granular surface	-42%	-36%	-62%	-55%	-73%	-66%	-79%	-74%
average	silo base level --> granular surface	-43%	-45%	-63%	-63%	-74%	-73%	-79%	-79%
4.40	wall upper edge	-34%	-	-53%	-	-63%	-	-72%	-
5.50	silo roof level	-18%	-	-40%	-	-53%	-	-62%	-

6.3 Dynamic overpressures

Figure 17 shows the maximum dynamic overpressure divided by the corresponding peak acceleration at the silo base level. Specifically, the ordinates provide the overpressures due to a unit silo base acceleration. It can be clearly seen that the pressure response of the upper cells (Cells 3 and 4) was always almost stable with all different inputs (except for the peak provoked by 0.2g random tests, namely Tests N. 180-182). The lower cells instead show some perturbations with all random inputs and multi-frequency sinusoidal inputs, while an almost stable response was observed over all tests. A qualitative comparison with the results from the fixed-based configuration (Figure 14 in Silvestri et al., 2022) indicates that the global response is somehow stable for all pressure cells with respect to the disturbed response from all tests in the fixed-based configuration. The quantitative comparison indicated an undoubtful reduction in the registered values as a consequence of the highly diminished acceleration values at the corresponding height of the pressure cells shown before. By summing all effects together, the isolation system is

able to globally regularize the internal induced dynamic internal forces removing the effect high peak acceleration values in terms of corresponding dynamic overpressure onto the silo wall.

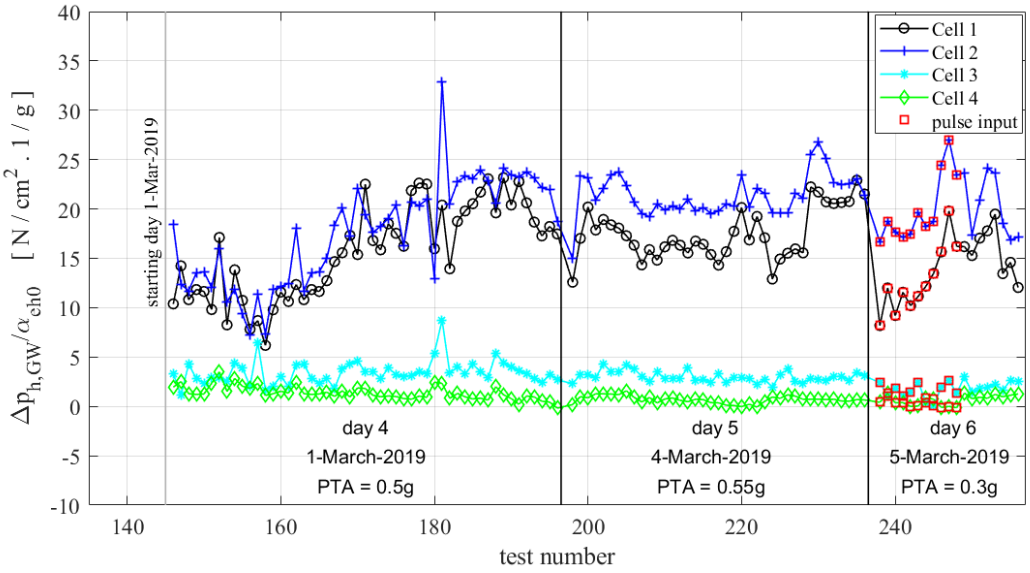

Figure 17: Dynamic overpressure/base acceleration ratio for each single test of the isolated-base configuration

Figure 18 (a and b) compare the dynamic overpressures measured at different acceleration levels of the pulse and the rs3 earthquake inputs. For each acceleration level, the black lines connect the mean value of the pressures measured by the two cells at the base level with that of the two cells at mid-height level within the granular solid, and these, in turn, with the zero value at the top surface of the granular solid. For both cases: (i) a clear qualitative trend of increasing dynamic overpressure value can be distinguished differently than Eurocode (EN 1998-4:2006 - [81]) and Trahair model predictions, the increment of the values between the two cells levels is in accordance with the Silvestri's model (not applicable in this case due to filling conditon limitation); (ii) the upper cells recorded a low values of overpressures with respect to the lower ones. That can be understood in the light of the variation of the acceleration profiles over the height (See figure 15) and the differences in the mass source (effective mass) between the two levels. The numerical values of the dynamic overpressures have shown a steep reduction with respect to the fixed-base configuration (Figure 15 in [11]). More in detail, Table 7 provides a numerical comparison of all values from the real earthquake tests rs3 and their correspondings from the first configurations (Figure 15b in Silvestri et al., 2022). It can be noticed the clear reduction seen before in the acceleration profiles at pressure cells levels is strongly relfected in the forces showing at least 82% reduction at the upper level (where less effective mass in involved) and a minimum value of 62% at the lower level of cells with an input characterized by 0.1 g nominal PTA. Those values increse with increasing acceleration where it can be definitely identified a maximum efficiency of the isolation system at high acceleration levels.

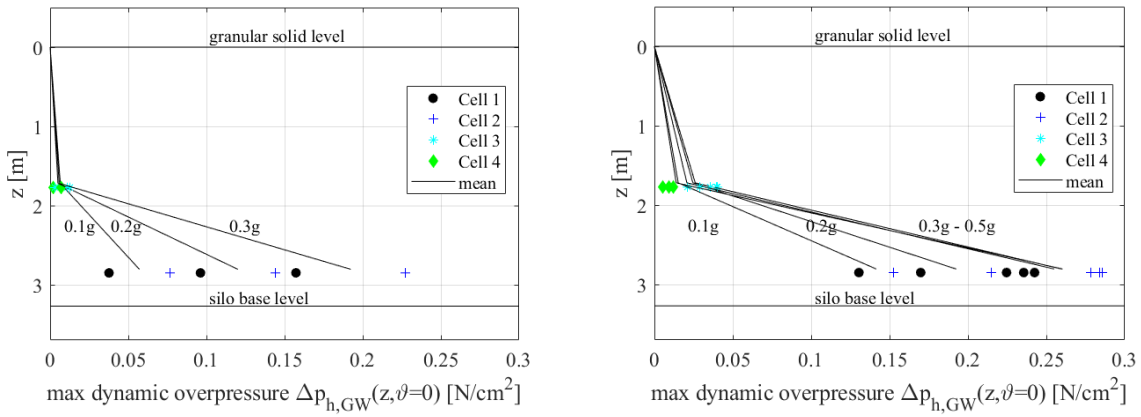

Figure 18: Maximum horizontal pressures measured by the four pressure cells for various (a) pulse and (b) earthquake tests.

Table 7: Induced dynamic overpressure differences between the fixed and isolated-base configuration with real earthquake input rs3.

Test	Nominal PTA	First level – 0.42 m		Second level – 1.5 m	
		Dynamic overpressure	Difference	Dynamic overpressure	Difference
[-]	[g]	[N/cm^2]	[%]	[N/cm^2]	[%]
19 (FIX)	0.1	0.369	-62%	0.099	-85%
201 (ISO)		0.141		0.015	
38 (FIX)	0.2	0.568	-66%	0.243	-90%
206 (ISO)		0.192		0.025	
55 (FIX)	0.3	0.749	-65%	0.361	-93%
211 (ISO)		0.259		0.026	
69 (FIX)	0.4	0.984	-74%	0.52	-96%
216 (ISO)		0.255		0.021	
86 (FIX)	0.5	1.453	-82%	0.861	-98%
222 (ISO)		0.26		0.014	

CONCLUDING REMARKS

The outcomes of a wide experimental campaign on a full-scale base-isolated flat-bottom filled silo system have been deeply analyzed, from both the isolation system and the superstructure response standpoints. Shaking table tests have been performed, by considering three individual typologies for input signals, namely sinusoidal, pulse-like and earthquake recordings.

Regarding the analysis of the adopted isolation system, the following conclusions are drawn:

- The harmonic tests have led to the proper evaluation of the commonly known cyclic effects of the frictional properties of Curved Surface Slider devices, with a decreasing value of friction coefficient with respect to the dissipated energy;

- The highlighted behavior can be easily modeled through an exponential decay curve, and consequently an analytical model of the whole isolation system can be accordingly defined;
- Even though a significantly simplified mechanical model has been implemented as representative of the overall structural system, the numerical simulations have returned a fairly good estimation of the experimental response returned by shaking table tests, regardless the input signals typology;
- The force response returned by the analytical model is actually able to reproduce the proper decay of frictional properties during motion, as a consequence of the heating phenomena which occur at all the sliding interfaces of the installed devices, and such agreement is automatically reflected also into the evaluation of the maximum displacement demand;
- Since the non-linear hysteretic rule has been implemented through an elasto-plastic model, the displacement experimental response is well captured by numerical simulations not only at the peak values, but also during the whole duration of the applied motions;
- Residual displacements are fairly estimated by the performed numerical Non-Linear Time History Analyses, especially for pulse-like ground motions, but also for harmonic and earthquake input signals.

Regarding the dynamic response of the filled silo system in isolated-base configuration and its comparison with the same system in fixed-based configuration, the following conclusions are drawn:

- A clear reduction in the acceleration magnitude was evidenced between the shaking table level and the silo base level. The efficiency of the isolation system tends to increase with increasing table acceleration, with a limited effect when the acceleration magnitude is lower than 0.10g (close to the friction value of the sliding surface of the isolators).
- Concerning the peak acceleration profiles along the height of the silo:
  -No clear amplification was observed under the effect of the pulse input or 0.1g multi frequency sinusoidal input;
  -The close-to-resonance input caused a maximum amplification of around 2 in the granular material close to the free surface and of around 1.5 in the silo wall at the same level.
- The dynamic overpressures due to unit silo base acceleration measurements show a somehow stable response for all inputs except for the random inputs, thus indicating a kind of robust regularization of the induced forces by the granular solid due the effect of the isolation system.
- The expected decrement in the magnitude for both accelerations and internal forces provided by the isolation system was quantified in the range of 30% to 80% depending on the input type, frequency content and acceleration magnitude.

ACKNOWLEDGEMENTS

The project ("SEismic Response of Actual steel SILOS (SERA-SILOS)", https://sera-ta.eucentre.it/index.php/sera-ta-project-18/) has received funding from the European Union's Horizon 2020 research and innovation program under grant agreement No 730900.

REFERENCES

[1] C. Maraveas, applied sciences Concrete Silos: Failures , Design Issues and Repair / Strengthening Methods, (2020).

[2] M. Khalil, S. Ruggieri, applied sciences Assessment of Structural Behavior , Vulnerability , and Risk of Industrial Silos : State-of-the-Art and Recent Research Trends, (2022).

[3] B. Kawecki, A. Halicka, J. Podgórski. Buckling of cylindrical concrete tanks and silos due to prestressing — nonlinear approach. Thin-Walled Struct (2022) 176: 109339.

[4] S. Mansour, L. Pieraccini, M. Palermo, D. Foti, G. Gasparini, Comprehensive Review on the Dynamic and Seismic Behavior of Flat-Bottom Cylindrical Silos Filled with Granular Material, Front. Built Enviroment. 7 (2022).

[5] M. Molenda, J. Horabik, I.J. Ross, M.D. Montross, Friction of wheat: grain-on-grain and on corrugated steel, Trans. Am. Soc. Agric. Eng. 45 (2002) 415–420.

[6] S. Mansour, S. Silvestri, A.J. Sadowski, the 'miniature silo' test: A simple experimental setup to estimate the effective friction coefficient between the granular solid and a horizontally-corrugated cylindrical metal silo wall, Powder Technol. 399 (2022) 117212.

[7] JH. Wood. Earthquake induced pressures on rigid wall structure. Bull NZ Soc Earthq Eng (1975) 8:175–86.

[8] NS. Trahair, A. Abel, P. Ansourian, HM. Irvine, JM. RotterStructural Design of Steel Bins for Bulk Solids (1983). Sydney, Australia: Australian Institute of Steel Construction, 30. ISBN 0909945357.

[9] S. Silvestri, G. Gasparini, T. Trombetti, D. Foti, On the evaluation of the horizontal forces produced by grain-like material inside silos during earthquakes, Bull. Earthq. Eng. 10 (2012) 1535–1560.

[10] S. Silvestri, S. Ivorra, L. Di Chiacchio, T. Trombetti, D. Foti, G. Gasparini, L. Pieraccini, M. Dietz, C. Taylor. Shaking-table tests of flat-bottom circular silos containing grain-like material. Earthquake Engng Struct. Dyn. (2016) 45:69–89.

[11] S. Silvestri, S Mansour, M. Marra et al., Shaking table tests of a full-scale flat-bottom manufactured steel silo filled with wheat: Main results on the fixed-base configuration, (2022) 51:169–190.

[12] A. Dogangun, Z. Karaca, A. Durmus, H. Sezen, Cause of Damage and Failures in Silo Structures, J. Perform. Constr. Facil. 23 (2009) 65–71.

[13] C. Fierro, E., Miranda, E., Perry, Behavior of Nonstructural Components in Recent Earthquakes, in: Archit. Eng. Conf., 2011: pp. 235–243. https://doi.org/https://doi.org/10.1061/41168(399)44.

[14] E. Uckan, B. Akbas, J. Shen, R. Wen, K. Turandar, M. Erdik, Seismic performance of elevated steel silos during Van earthquake, October 23, 2011, Nat. Hazards. 75 (2015) 265–287.

[15] E. Azre, Seismic Deisgn Practices of Industries, in: Earthq. Eng. Proc. Tenth World Conf. Balkema, Rotterdam, 1992: pp. 5019–5023.

[16] E. Arze, Seismic design of industrial facilities, Tectonophysics. 218 (1993) 23–41.

[17] PI. Griffin, MJ. Bragagnolo, LJ. Yanev, The December 7,1988 Armenia earthquake effects on selected power, industrial and commercial facilities(1995).

[18] N. Augenti, A. Nanni, F. Parisi, Construction failures and innovative retrofitting, Buildings. 3 (2013) 100–121.

[19] V. Gioncu, FM. Mazzolani. Seismic Design of Steel Structures. 2014 Florida, United States: CRC Press. ISBN 9781138075375.

[20] S. Grimaz. Can earthquakes trigger serious industrial accidents in Italy? Some considerations following the experiences of 2009 L'Aquila (Italy) and 2012 Emilia (Italy) earthquakes, Boll. Di Geofis. Teor. Ed Appl. 55 (2014) 227–237.

[21] F. Villalobos, M. Mendoza, Damages observed in the 2010 Concepción earthquake related to soil phenomena, 5th Int. Conf. Earthq. Geotech. Eng. (2011).

[22] P. Grossi, C. Williams, C. Cabrera, T. Tabucchi, P. Sarabandi, A. Rodríguez, H. Aslani, M. Rahnama, The 2010 Maule, Chile Earthquake: Lessons and Future Challenges, Risk Manag. Solut. Inc. (2010) 1–46.

[23] C. Butenweg, J. Rosin, S. Holler Analysis of Cylindrical Granular Material Silos under Seismic Excitation. Buildings (2017) 7.

[24] JM. Rotter, TS. Hull. Wall loads in squat steel silos during earthquakes, Eng. Struct. 11 (1989) 139–147.

[25] L. Pieraccini, S. Silvestri, T. Trombetti, Refinements to the Silvestri's theory for the evaluation of the seismic actions in flat-bottom silos containing grain-like material, Bull. Earthq. Eng. 13 (2015) 3493–3525.

[26] A. Durmuş, R. Livaoğlu, A simplified 3 D.O.F. model of A FEM model for seismic analysis of a silo containing elastic material accounting for soil-structure interaction, Soil Dyn. Earthq. Eng. 77 (2015) 1–14.

[27] R Livaoğlu, A Durmuş. Investigation of wall Flexibility Effects on Seismic Behavior of Cylindrical Silos. Struct. Eng. Mech. 53 (2015).

[28] H. Zhang, K. Han, J. Yang, L. Chen. Experimental and Numerical Investigation of Plastic–Concrete Waterproof Walls of an Underground Granary Subject to Combined Bending Moment and Water Pressure. Buildings (2022) 12: 893

[29] S.J. Lee, Experimental study of cylindrical silos subject to seismic excitation. A PhD thesis - The Ohio State University, 1981.

[30] A. Yokota, H., Sugita, M., & Mita, Vibration tests and analyses of coal-silo model, in: Proc., 2nd Int. Conf. Des. Silos Strength Flow, Strat. Powder Advis. Cent., (1983) 107–116.

[31] A Shimamoto, M Kodama, M Yamamura. Vibration Tests for Scale Model of Cylindrical Coal Storing Silo, in Proceedings of the 8th World Conference on Earthquake Engineering (1984- Hoboken, New Jersey, United States: Prentice-Hall), 5, 287–294.

[32] EC. Harris, JD. Von Nad. Experimental Determination of Effective Weight of Stored Material for Use in Seismic Design of Silos. ACI J. Proc. (1985) 828–833.

[33] J. Sasaki, Y., Yoshimura, Dynamic Behavior of Concrete Stave Silos.pdf, in: Proc. 8th World Conf. Earthq. Eng., 1984: pp. 937–944.

[34] J. Sasaki, Y., Yoshimura, Dynamic Behavior of Concrete Stave Silos.pdf, in: Proc. 8th World Conf. Earthq. Eng., 1988: pp. 937–944.

[35] J. Sasaki, Y., Yoshimura, Dynamic discrete modeling and computer simulation of seismic esponse of concrete stave silos with structural discontinuity, in: Earthq. Eng. Proc. Tenth World Conf. Balkema, Rotterdam, 1992: pp. 5065–6070.

[36] Y. Naito, Equivalent linear technique in the finite element method applied to deformation with volume change and to an axisymmetric body under an unaxisymmetric load, Proc. 9th World Conf. (1988) 133–138.

[37] S. Holler, K. Meskouris, Granular Material Silos under Dynamic Excitation: Numerical Simulation and Experimental Validation, J. Struct. Eng. 132 (2006) 1573–1579.

[38] R. Tatko, S. Kobielak, Horizontal bulk material pressure in silo subjected to impulsive load, Shock Vib. 15 (2008) 543–550.

[39] L. Shuwei, Z. Wen, G. Zhiyu, O. Access, Study on dynamic characteristics of silo-stock-foundation interaction system under seismic load, (2018) 435–440.

[40] Q. Xu, Q. Liu, Seismic analysis on reinforced concrete group silos through shaking table tests, (2020) 1–12.

[41] H. Jing, H. Chen, J. Yang, P. Li, Shaking table tests on a small-scale steel cylindrical silo model in different filling conditions, Structures. 37 (2022) 698–708.

[42] E. Uckan, B. Akbas, J. Shen, R. Wen, K. Turandar, M. Erdik, Seismic performance of elevated steel silos during Van earthquake, October 23, 2011, Nat. Hazards. 75 (2015) 265–287.

[43] K Guo, C Zhou, L Meng, X Zhang. Seismic vulnerability assessment of reinforced concrete silo considering granular material-structure interaction. Struct. Des. Tall Spec. Build (2016) 25: 1011-1030.

[44] F. Morelli, R. Laguardia, M. Faggella, Ground motions and scaling techniques for 3D performance based seismic assessment of an industrial steel structure, Bull. Earthq. Eng. 16 (2018) 1179–1208.

[45] S. Benkhellat, O. Kada, A. Seghir, M. Kadri. Seismic damage assessment of reinforced concrete grain silos. International Journal of Structural Stability and Dynamics (2022) 22, No. 01, 2250005.

[46] A.M. Mehretehran, S. Maleki, Thin-Walled Structures 3D buckling assessment of cylindrical steel silos of uniform thickness under seismic action, Thin Walled Struct. 131 (2018) 654–667.

[47] A.M. Mehretehran, S. Maleki, Axial buckling of imperfect cylindrical steel silos with isotropic walls under stored solids loads: FE analyses versus Eurocode provisions, Eng. Fail. Anal. 137 (2022) 106282.

[48] P Trávníček, L Kotek, P Junga. Prevention of accidents in facilities for the treatment and storage of selected agricultural products, 153 (2022).

[49] F. Morelli, A. Piscini, W. Salvatore, Seismic behavior of an industrial steel structure retrofitted with self-centering hysteretic dampers, J. Constr. Steel Res. 139 (2017) 157–175.

[50] D Bîtcă, E Ursu, P Ioan. Engineering, seismic base isolators for a silo supporting structure, 11 (2015) 1–9.

[51] A. Kanyilmaz, C.A. Castiglioni, Simplified Numerical Modeling of Elevated Silos for Nonlinear Dynamic Analysis, Ing. Sismica. 33 (2015) 5–14.

[52] A. Kanyilmaz, C.A. Castiglioni, J. Georgi, SEISMIC RETROFIT OF INDUSTRIAL SILOS BY MEANS OF BASE, (2016) 5–10.

[53] E. Rossi, M. Ventrella, M. Faggella, R. Gigliotti, I.D. Analyses, Performance based earthquake assessment of an industrial silos structure and retrofit with sliding, (2016) 5–10.

[54] A. Kanyilmaz, C.A. Castiglioni, Reducing the seismic vulnerability of existing elevated silos by means of base isolation devices, Eng. Struct. 143 (2017) 477–497.

[55] P.P.A. Vimal, J.D.J. Regin, Experimental investigation on elevated water tanks with base isolation – response spectrum approach Paul P.A. Vimal, Joseph D.J. Regin, (2020) 885–899.

[56] M. Moslemi, M.R. Kianoush, Application of seismic isolation technique to partially filled conical elevated tanks, Eng. Struct. 127 (2016) 663–675.

[57] M.E. Compagnoni, O. Curadelli, D. Ambrosini, Journal of Loss Prevention in the Process Industries Experimental study on the seismic response of liquid storage tanks with Sliding Concave Bearings, J. Loss Prev. Process Ind. 55 (2018) 1–9.

[58] A. Krishnamoorthy, Finite Element Method of Analysis for Liquid Storage Tank Isolated with Friction Pendulum System, J. Earthq. Eng. 00 (2018) 1–11.

[59] A. Tsipianitis, Y. Tsompanakis, Seismic Vulnerability Assessment of Liquid Storage Tanks Isolated by Sliding-Based Systems, 2018 (2018).

[60] A. Tsipianitis, Y. Tsompanakis, Impact of damping modeling on the seismic response of base-isolated liquid storage tanks, Soil Dyn. Earthq. Eng. 121 (2019) 281–292.

[61] W Jing, P Chen, Y Song. Shock absorption of concrete liquid storage tank with different kinds of isolation measures. Earthquakes and Structures (2020) 18: 467-480

[62] Z. Zhao, X. Lu, Y. Guo, X. Zhao, Seismic Fragility Assessment of Base-Isolated Steel Water Storage Tank, (2020) 8835943.

[63] D. Hernandez-Hernandez, T. Larkin, N. Chouw. Shake table investigation of nonlinear soil–structure–fluid interaction of a thin-walled storage tank under earthquake load. Thin-Walled Struct (2021) 167:108143.

[64] A. Tsipianitis, Y. Tsompanakis, Optimizing the seismic response of base-isolated liquid storage tanks using swarm intelligence algorithms, Comput. Struct. 243 (2021) 106407.

[65] E. Güler, C. Alhan, Performance limits of base-isolated liquid storage tanks with / without supplemental dampers under near-fault earthquakes, Structures. 33 (2021) 355–367.

[66] A. Tsipianitis, Y. Tsompanakis, Improving the seismic performance of base-isolated liquid storage tanks with supplemental linear viscous dampers, 21 (2022) 269–282.

[67] SI. Reyes, JL. Almazán, MF. Vassiliou, NF. Tapia, JI. Colombo, JC. de la Llera. Full-scale shaking table test and numerical modeling of a 3000-liter legged storage tank isolated with a vertical rocking isolation system. Earthquake Engng Struct Dyn. (2022) 51:1563–1585.

[68] JI. Colombo, JL. Almazán. Experimental investigation on the seismic isolation for a legged wine storage tankJournal of Constructional Steel Research (2017) 133: 167-180.

[69] PPA. Vimal., JDJ. Regin, GTR. Jinu, CG. Chettiar. Experimental investigation on elevated water tanks with base isolation – response spectrum approach. Journal of Theoretical and Applied Mechanics (2020) 58: 885-899.

[70] Butenweg C.,Holtschoppen B. (2014) Seismic Design of Industrial Facilities in Germany, Seismic Design of Industrial Facilities, DOI: 10.1007/978-3-658-02810-7_6

[71] Kammerer A., Whittaker A., Constantinou M.C. (2019) Technical considerations for seismic isolation of nuclear facilities, Report number: NUREG/CR-7253, Affiliation: U.S. Nuclear Regulatory Commission

[72] Mazza F., (2017) Lateral-torsional response of base-isolated buildings with curved surface sliding system subjected to near-fault earthquakes, Mechanical Systems and Signal Processing, 92 (2017) 64–85.

[73] Weber F. (2014) Semi-active vibration absorber based on real-time controlled MR damper, Mechanical Systems and Signal Processing, 46 (2014) 272–288.

[74] Tomita N., Hase Y., Fujita S., Okamura S. (2016) Study on response characteristics of seismically isolated structures intended for industrial facilities, January 2016The Proceedings of the Dynamics & Design Conference 2016:213, DOI: 10.1299/jsmedmc.2016.213

[75] Marti J., Crespo M.J., Martínez F. (2010) Seismic isolation of liquefied natural gas tanks: A comparative assessment, Seismic Isolation and Protective Systems 1(1):125-140, DOI: 10.2140/siaps.2010.1.125

[76] Kotrasova K., Kormanikova E., Loukili M., Mansour S. and Foti D. (2022). The seismic response of cylindrical steel tank at Al Hoceïma city in Morocco. 2022 IOP Conf. Ser.: Mater. Sci. Eng. 1252 012014 (2022). DOI: 10.1088/1757-899X/1252/1/012014

[77] CEN [2009], Comité Européen de Normalisation TC 340, European Code UNI EN 15129:2009 Anti-seismic devices, European Committee for Standardization, Brussels, Belgium.

[78] AASHTO [2014] Guide Specifications for Seismic Isolation Design, American Association of State Highway and Transportation Officials, Washington, DC.

[79] M. Furinghetti, A. Pavese, V. Quaglini, P. Dubini. Experimental Investigation of The Cyclic Response of Double Curved Surface Sliders Subjected To Radial And Bidirectional Sliding Motions, Soil Dynamics and Earthquake Engineering (2019). DOI: 10.1016/j.soildyn.2018.11.020

[80] V. Quaglini, P. Dubini, M. Furinghetti, A. Pavese. Assessment of Scale Effects in the Experimental Evaluation of the Coefficient of Friction of Sliding Isolators, Journal of Earthquake Engineering (2019). DOI: 10.1080/13632469.2019.1687054.

[81] EN 1998-4: 2006. Eurocode 8. Design of structures for earthquake resistance, Part 4 -Silos, tanks and pipelines, CEN, Brussels.

[82] Pavese A., Furinghetti M., Casarotti C. (2018) “Experimental Assessment of the Cyclic Response of Friction-Based Isolators under Bidirectional Motions,” Soil Dynamics and Earthquake Engineering, DOI: 10.1016/j.soildyn.2018.06.031.